Journal of Applied Physics

Introduction to antiferromagnetic magnons

Cite as: J. Appl. Phys. **126**, 151101 (2019); https://doi.org/10.1063/1.5109132
Submitted: 06 May 2019 • Accepted: 22 September 2019 • Published Online: 15 October 2019

Sergio M. Rezende, Antonio Azevedo and Roberto L. Rodríguez-Suárez

AIP Publishing

Journal of Applied Physics TUTORIAL scitation.org/journal/jap

Introduction to antiferromagnetic magnons

Cite as: J. Appl. Phys. **126**, 151101 (2019); doi: 10.1063/1.5109132
Submitted: 6 May 2019 · Accepted: 22 September 2019 ·
Published Online: 15 October 2019

Sergio M. Rezende,[1,a)] Antonio Azevedo,[1] and Roberto L. Rodríguez-Suárez[2]

AFFILIATIONS

[1]Departamento de Física, Universidade Federal de Pernambuco, 50670-901, Recife, Pernambuco, Brazil
[2]Facultad de Física, Pontifícia Universidad Católica de Chile, Casilla 306, Santiago, Chile

[a)]**Author to whom correspondence should be addressed:** rezende@df.ufpe.br

ABSTRACT

The elementary spin excitations in strongly magnetic materials are collective spin deviations, or spin waves, whose quanta are called magnons. Interest in the experimental and theoretical investigation of magnons attracted many groups worldwide about 4–6 decades ago and then waned for some time. In recent years, with the advent of the field of spintronics, the area of magnonics has gained renewed attention. New phenomena have been discovered experimentally, and others have been predicted theoretically. In this tutorial, we briefly review the basic concepts of magnons in antiferromagnetic (AF) materials. Initially, we present a semiclassical view of the equilibrium spin configurations and of the antiferromagnetic resonance in AF materials with two types of magnetic anisotropy, easy-axis and easy-plane. Then, we present a quantum theory of magnons for these materials and apply the results to two important AF insulators, MnF_2 and NiO. Finally, we introduce the concept of antiferromagnetic magnonic spin current that plays a key role in several phenomena in antiferromagnetic spintronics.

I. INTRODUCTION

Antiferromagnets are magnetic materials that have no net macroscopic magnetization and, therefore, are almost insensitive to external magnetic fields. The existence of antiferromagnetism was proposed by Louis Néel[1] to account for the magnetic behavior of some salts with complicated lattice structures. Néel first assumed that the ordered magnetic arrangements could be described in terms of "spin sublattices," each having all spins aligned in the same direction. Then, he considered that the interaction between the spins in different sublattices could be negative so that they would be aligned antiparallel. Now we know that the coupling between spins originates mainly in the exchange interaction, with magnitude represented by an exchange parameter J. The intrasublattice J is positive because it is due to direct exchange, while the intersublattice J is negative because it arises from the superexchange that is mediated by ligand ions between the magnetic ions. If the sublattices have different magnetizations, the materials are called "ferrimagnets," which have spontaneous net magnetization below the ordering temperature T_c and in many respects behave like ferromagnets. Materials with $J < 0$ that have sublattices with the same magnetization are called "antiferromagnets." In the ordered phase, below a critical temperature called Néel temperature T_N, they are magnetic but have no net macroscopic magnetization.

In his 1970 Nobel lecture, Louis Néel[2] stated that "Antiferromagnetic materials are extremely interesting from the theoretical viewpoint, but do not seem to have any application." This pessimistic view of antiferromagnets would change dramatically a few decades later. Today, these materials have practical applications and promise to deliver several more. The debut of antiferromagnets in technology was made possible with the discovery of the giant magnetoresistance effect (GMR) in 1988 by Albert Fert[3] and Peter Grünberg.[4] They showed that in magnetic structures with nanometer thick multilayers, the electron transport could be controlled by the spin instead of the electric charge as in conventional electronics. This discovery triggered research in magnetic multilayers and gave birth to the field of spintronics, which has revolutionized magnetic recording technologies and promises new functionalities to electronic devices.

Antiferromagnetic materials proved to be essential in GMR sensors for pinning the magnetization of a reference ferromagnetic layer by means of the exchange bias phenomenon.[5–7] Since the late 1990s, disk-drive magnetic read-heads are based on GMR sensors that are much more sensitive to changes in magnetic fields than the traditional induction heads. Although important, antiferromagnetic (AF) materials have had a passive role in spintronic devices; the active role is played by ferromagnetic materials. However, in recent

years, this scenario began to change with new experimental and theoretical results showing that antiferromagnets have several advantages over ferromagnets in spintronic phenomena. One of them is the fact that AF materials are insensitive to external magnetic perturbations. Another one is the ultrafast dynamics of antiferromagnets that promise device operation in the terahertz frequency range. These late developments gave rise to the field of antiferromagnetic spintronics.[8–14]

In this tutorial, we review the basic concepts and properties of the collective spin excitations in antiferromagnets, the spin waves, whose quanta are called magnons. Antiferromagnets are known to exist with a great variety of crystalline structures and physical properties, and new materials continue to be discovered.[13] Here, we will restrict attention to simple AF insulators with only two sublattices, one class with uniaxial magnetic anisotropy, also called easy-axis anisotropy, such as the fluorides MnF_2 and FeF_2, and the other with two anisotropy axes, or easy-plane anisotropy, such as the oxides NiO and MnO.

II. SPIN CONFIGURATIONS IN SIMPLE ANTIFERROMAGNETS

We consider initially two simple antiferromagnets with uniaxial, or easy-axis, anisotropy, MnF_2 and FeF_2. Both have the rutile crystal structure, a body-centered tetragonal lattice with the magnetic ions occupying the corner and body-centered positions, as shown in Fig. 1(a).[15] Below the Néel temperature, 66.5 K for MnF_2 and 78.4 K for FeF_2, and in the absence of an external magnetic field, the spins are arranged in two oppositely directed sublattices, pointing along the easy anisotropy direction (c axis). The magnetic properties are described very well by a Hamiltonian consisting of contributions from Zeeman, exchange, and magnetic anisotropy energies in the form[16–19]

$$\mathrm{H} = -\gamma\hbar\sum_i \vec{H}_0\cdot\vec{S}_i + \sum_{i,i'\neq i} 2J_{ii'}\,\vec{S}_i\cdot\vec{S}_{i'} - D\sum_i (S_i^z)^2, \qquad (1)$$

where $\gamma = g\mu_B/\hbar$ is the gyromagnetic ratio, g is the spectroscopic splitting factor, μ_B is the Bohr magneton, $\hbar$ is the reduced Plank constant, $\vec{S}_i$ is the spin (in units of $\hbar$) at a generic lattice site i, $\vec{H}_0$ is the applied magnetic field, $J_{ii'}$ is the exchange constant of the interaction between spins $\vec{S}_i$ and $\vec{S}_{i'}$ and D is the uniaxial anisotropy constant. The important exchange interactions are illustrated in Fig. 1(a). In MnF_2, the exchange parameters determined by inelastic neutron scattering measurements[19] are $J_1 = 0.028$ meV, $J_2 = -0.152$ meV, and $J_3 = -0.004$ meV. Thus, the negative intersublattice J_2 is the dominant interaction and determines the antiferromagnetic arrangement of the sublattices.

In order to find the spin equilibrium configuration, we use a macrospin approximation and associate to $\vec{S}_i$ and $\vec{S}_j$ the uniform sublattice magnetizations in sublattices 1 and 2, respectively, given by $\vec{M}_{1,2} = \gamma\hbar N\vec{S}_{i,j}$, where N is the number of spins per unit volume. For $T = 0$, the static sublattice magnetizations have the same value, $M_1 = M_2 = M$. Considering a magnetic field H_0 applied along the c axis, the z-direction of the system shown in Fig. 1, from Eq. (1), we have the energy per unit volume

$$E = -H_0(M_{1z} + M_{2z}) + \frac{H_E}{M}\vec{M}_1\cdot\vec{M}_2 - \frac{H_A}{2M}(M_{1z}^2 + M_{2z}^2), \qquad (2)$$

where H_E and H_A are the effective exchange and anisotropy fields defined by

$$H_E = 2SzJ_2/\gamma\hbar, \quad H_A = 2SD/\gamma\hbar, \qquad (3)$$

where we have considered only intersublattice exchange interaction between the z nearest neighbors. Due to the symmetry, the sublattice magnetizations and the applied field are in the same plane so that the energy in Eq. (2) becomes

$$\frac{E(\theta_1,\theta_2)}{M} = -H_0(\cos\theta_1 + \cos\theta_2) + H_E\cos(\theta_1+\theta_2) - \frac{H_A}{2}(\cos^2\theta_1 + \cos^2\theta_2), \qquad (4)$$

where θ_1 and θ_2 are the polar angles of the corresponding sublattice magnetizations. The conditions $\partial E/\partial\theta_1 = \partial E/\partial\theta_2 = 0$ give two possible equilibrium configurations. As illustrated in Fig. 1(b), $\theta_1 = 0$, $\theta_2 = \pi$ corresponds to the antiferromagnetic (AF) phase, while $\theta_1 = \theta_2 = \cos^{-1}[H_0/(2H_E - H_A)]$ corresponds to the spin-flop (SF) phase. Substitution of these angles in Eq. (4) shows that the AF phase has lower energy for fields $H_0 < H_{SF}$, while the SF phase has lower energy for $H_0 > H_{SF}$, where $H_{SF} = (2H_EH_A - H_A^2)^{1/2}$. For

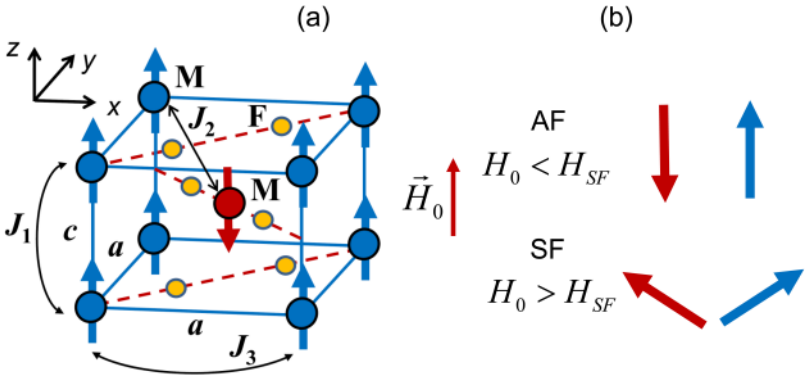

FIG. 1. (a) Crystal structure of the easy-axis rutile antiferromagnets MnF_2 and FeF_2. The ions M represent Mn^{2+} or Fe^{2+}. (b) Spin configurations in the antiferromagnetic (AF) and spin flop (SF) phases with the external field applied along the easy axis.

small fields applied in the z-direction, the spins are along the c axis in the AF phase. As the field intensity increases and reaches H_{SF}, the system undergoes a first-order phase transition to the SF phase.

The magnetic interactions in MnF_2 and FeF_2 are dominated by nearest-neighbor exchange, having comparable intersublattice exchange fields, respectively, $H_E = 526\,\text{kOe}$ and $H_E = 540\,\text{kOe}$.[15] In MnF_2, the ground state configuration of the magnetic Mn^{2+} ions is $3d^5(^6S_{5/2})$, which has no orbital angular momentum so that it has very small single-ion anisotropy. The origin of the magnetic anisotropy of MnF_2 relies mainly in the dipolar interaction, with a relatively small effective anisotropy field $H_A = 8.2\,\text{kOe}$[19,20] so that $H_{SF} \approx (2H_EH_A)^{1/2} = 93\,\text{kOe}$. The temperature dependence of the spin-flop field has been measured by ultrasonic techniques,[21] antiferromagnetic resonance,[22] and spin Seebeck effect.[23] In FeF_2, the ground state configuration of the magnetic Fe^{2+} ions is $3d^5(^5D_4)$, which has a finite orbital angular momentum, resulting in a large effective anisotropy field $H_A = 200\,\text{kOe}$ arising from the spin-orbit coupling.[24,25] Thus, the spin-flop field is large, $H_{SF} = 505\,\text{kOe}$, and can be attained only with pulsed magnetic fields.[26]

The other material we will investigate here is NiO, which, due to its simple structure and spin interactions, is considered a prototypical room-temperature antiferromagnetic insulator. Its magnetic structure and spin interactions are similar to those in MnO.[27,28] This material has been extensively used in experimental investigations of many phenomena, such as exchange bias,[5–7,29–31] inelastic light scattering,[32,33] and magnetic response at terahertz frequencies.[34–36] More recently, it has been shown that a thin layer of NiO in spintronic devices can be used to transport a magnonic spin current while blocking charge current.[37–42] Also, NiO has the potential to generate radiation with terahertz frequency in spin-torque nano-oscillators,[43] and under a thermal gradient it exhibits the spin Seebeck effect at room temperature.[44]

In the paramagnetic phase, NiO has the face-centered cubic structure of sodium chloride. Below the Néel temperature $T_N \approx 523\,\text{K}$, the Ni^{2+} spins are ordered ferromagnetically in {111} planes, lying along $\langle 11\bar{2}\rangle$ axes, with adjacent planes oppositely magnetized due to a super-exchange AF interaction, as illustrated in Fig. 2. It is characterized by two distinct anisotropies, a negative one (hard) along $\langle 111\rangle$ axes that forces the spins into the {111} planes, and a positive (easy) in-plane one along $\langle 11\bar{2}\rangle$ axes. The spin Hamiltonian with Zeeman energy, exchange interaction energy, and out-of-plane (x) and in-plane (z) anisotropy energies can be written as[28]

$$\mathrm{H} = -\gamma\hbar \sum_{i,j} \vec{H}_0 \cdot \vec{S}_{i,j} + \sum_{i,j} 2J_{ij}\,\vec{S}_i \cdot \vec{S}_j + \sum_{i,j} D_x (S^x_{i,j})^2 - D_z (S^{z'}_{i,j})^2 . \tag{5}$$

The difference to Eq. (1) is that the Hamiltonian now contains two anisotropy terms, with anisotropy constants D_x and D_z. Both are taken to be positive so that the signs in Eq. (5) imply that x is a hard direction along a $\langle 111\rangle$ axis, while z' are easy directions along $\langle 11\bar{2}\rangle$ axes. Since there are three equivalent directions in the easy-plane and four {111} planes, in bulk NiO crystals there are AF domains with spins in 12 different directions, which complicates the interpretation of some magnetic measurements.[45,46]

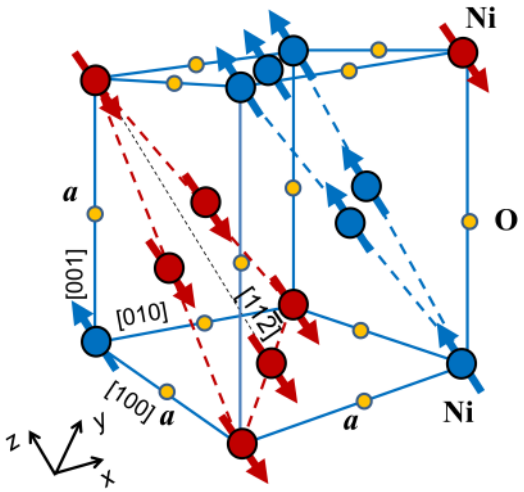

FIG. 2. Crystal structure and spin arrangements in the easy-plane antiferromagnet NiO. The small yellow circles represent O^{2-} ions and the large circles represent the Ni^{2+} ions.

Considering the external field applied along one of the z'-directions in the {111} plane, with Eq. (5), we obtain for the energy per unit volume

$$E = -H_0(M_{1z'} + M_{2z'}) + \frac{H_E}{M}\vec{M}_1 \cdot \vec{M}_2 + \frac{H_{Ax}}{2M}(M^2_{1x} + M^2_{2x}) - \frac{H_{Az}}{2M}(M^2_{1z'} + M^2_{2z'}), \tag{6}$$

where, with the relevant intersublattice exchange constant, the effective exchange field is given by the same expression as in Eq. (3), but now we have two anisotropy fields

$$H_{Ax} = 2S\,D_x/\gamma\hbar, \quad H_{Az} = 2S\,D_z/\gamma\hbar. \tag{7}$$

In order to simplify calculations, we assume a monodomain sample with the field applied along an easy direction. In this case, $M_{1x} = M_{2x} = 0$ and Eq. (6) reduces to Eq. (2) so that the result previously obtained is valid here. In NiO, the effective fields are $H_E = 9\,684\,\text{kOe}$, $H_{Ax} = 6.35\,\text{kOe}$, $H_{Az} = 0.11\,\text{kOe}$ so that the field for the spin-flop transition $H_{SF} = \sqrt{2H_EH_{Az}}$ is 46.3 kOe.[47]

III. ANTIFERROMAGNETIC RESONANCE: THE $k = 0$ MAGNONS

We now derive the resonance frequencies of the uniform precession modes of the sublattice magnetizations, which correspond to the magnons with zero wave vector. The equations of motion for the magnetization components are obtained from the Landau–Lifshitz equation

$$\frac{d\vec{M}_{1,2}}{dt} = \gamma\vec{M}_{1,2} \times \vec{H}_{eff\,1,2}, \tag{8}$$

where $\vec{H}_{eff\,1,2}$ represent the effective fields that act on the sublattice magnetizations, given by

$$\vec{H}_{eff\,1,2} = -\nabla_{\vec{M}1,2}[E(\vec{M}_{1,2})]. \tag{9}$$

Since the uniaxial antiferromagnet is a particular case of the biaxial AF, we will consider the energy in Eq. (6), with the static field applied along a direction of equilibrium so that the result can be used for both easy-axis and easy-plane AFs. Writing for the magnetizations $\vec{M}_{1,2} = \hat{z}\,M_{1,2z} + (\hat{x}\,m_{1,2x} + \hat{y}\,m_{1,2y})\,e^{-i\omega t}$, we obtain with Eqs. (8) and (9) the linearized equations of motion for the transverse components of the sublattice magnetizations

$$i\omega\, m_{1x} + \gamma\, m_{1y}(H_0 + H_E + H_{Az}) + \gamma\, H_E m_{2y} = 0, \tag{10a}$$

$$-\gamma\, m_{1x}(H_0 + H_E + H_{Ax} + H_{Az}) + i\omega\, m_{1y} - \gamma\, H_E m_{2x} = 0, \tag{10b}$$

$$-\gamma\, H_E m_{1y} + i\omega\, m_{2x} + \gamma\, m_{2y}\,(H_0 - H_E - H_{Az}) = 0, \tag{10c}$$

$$+\gamma\, H_E m_{1x} - \gamma\, m_{2x}(H_0 - H_E - H_{Ax} - H_{Az}) + i\omega\, m_{2y} = 0, \tag{10d}$$

where we have considered $M_{1z} = M$, $M_{2z} = -M$. The antiferromagnetic resonance (AFMR) frequencies are the eigenvalues of the resonance matrix $[A]$, given by

$$[A] = \begin{bmatrix} 0 & 0 & -\gamma H_0 - (A - C) & -B \\ 0 & 0 & B & -\gamma H_0 + (A - C) \\ -\gamma H_0 - (A + C) & -B & 0 & 0 \\ B & -\gamma H_0 + (A + C) & 0 & 0 \end{bmatrix}, \tag{11}$$

where the parameters are

$$A = \gamma\,(H_E + H_{Ax}/2 + H_{Az}), \quad B = \gamma\, H_E, \quad C = \gamma\, H_{Ax}/2. \tag{12}$$

Equations (10) can be written as an eigenvalue equation in matrix form

$$[A][S] = [S][\omega], \tag{13}$$

where the columns of [S] are eigenvectors of [A] that represent the four normal modes with components $(m) = (m_{1x}, m_{2x}, im_{1y}, im_{2y})^T$, and $[\omega]$ is the diagonal matrix of the eigenvalues, which are given by the roots of

$$\det\{[A] - [\omega]\} = 0. \tag{14}$$

Note that the problem can also be formulated with the equations of motion for the Néel vector $\vec{l} = \vec{m}_1 - \vec{m}_2$ and the total small-signal magnetization $\vec{m} = \vec{m}_1 + \vec{m}_2$.[43]

A. Easy-axis antiferromagnets

Initially, we apply the results for the case of easy-axis AFs by setting $H_{Ax} = 0$. The solution of Eq. (14) with $C = 0$ gives for the AFMR frequencies (eigenvalues)[16]

$$\omega_1 = -\omega_2 = \gamma H_0 + \sqrt{A^2 - B^2}, \tag{15a}$$

$$\omega_3 = -\omega_4 = \gamma H_0 - \sqrt{A^2 - B^2}. \tag{15b}$$

We shall use α to denote modes 1 and 2, and β for modes 3 and 4. From Eqs. (12) and (15), the positive frequencies for the two modes are

$$\omega_{\alpha,\beta} = \gamma(H_c \pm H_0), \tag{16}$$

where

$$H_c = (2H_E H_A + H_A^2)^{1/2}, \quad H_A = H_{Az}. \tag{17}$$

Thus, the two modes are degenerate in the absence of an external magnetic field. The application of an external field H_0 in the direction of the anisotropy lifts the degeneracy. Equation (16) shows that the frequency of mode α increases with an increasing field, while the frequency of mode β decreases with an increasing field. In order to characterize the behavior of the sublattice magnetizations in the AFMR, one has to solve the full eigenvalue equation. For $H_0 = 0$, it can be shown that Eq. (13) is satisfied by the eigenvector matrix[16]

$$[S] = \begin{bmatrix} \eta_\alpha & -\eta_\alpha & \eta_\beta & -\eta_\beta \\ -1 & 1 & -1 & 1 \\ -\eta_\alpha & -\eta_\alpha & -\eta_\beta & -\eta_\beta \\ 1 & 1 & 1 & 1 \end{bmatrix}, \tag{18}$$

where

$$\eta_\alpha = \frac{H_E + H_A + H_c}{H_E}, \quad \eta_\beta = \frac{H_E + H_A - H_c}{H_E}. \tag{19}$$

Hence, the components of the sublattice magnetizations in the two modes are

$$\begin{pmatrix} m_{1x} \\ m_{2x} \\ im_{1y} \\ im_{2y} \end{pmatrix}_\alpha = A_\alpha \begin{pmatrix} \eta_\alpha \\ -1 \\ -\eta_\alpha \\ 1 \end{pmatrix}, \quad \begin{pmatrix} m_{1x} \\ m_{2x} \\ im_{1y} \\ im_{2y} \end{pmatrix}_\beta = A_\beta \begin{pmatrix} -\eta_\beta \\ 1 \\ -\eta_\beta \\ 1 \end{pmatrix}, \tag{20}$$

where A_α and A_β are amplitude factors that depend on the driving field. Equations (20) show that the two sublattice magnetizations are nearly opposite to each other, and they precess circularly in the same sense, counterclockwise in mode α and clockwise in mode β. In the α-mode, the ratio between the precession amplitudes of the two sublattices is $m_{1x}/m_{2x} = -\eta_\alpha$, which is larger than unity in absolute value. Thus, the angle of $\vec{M}_1$ with the z axis is larger than the angle of $\vec{M}_2$, as illustrated in Fig. 3 (a). On the other hand, in the β -mode, $m_{1x}/m_{2x} = -\eta_\beta$, which is smaller than unity in absolute value, showing that the angle of $\vec{M}_1$ with the z axis is smaller than the angle of $\vec{M}_2$, as in Fig. 3(a).

Note that the effect of the anisotropy field is enhanced by the interplay with exchange, and this gives rise to the gap in the spectrum. The opposite directions of the anisotropy fields for the two sublattice magnetizations make it impossible for them to precess in the same direction, and this brings the exchange field into play. The interplay between the anisotropy and the large exchange interaction results in a magnetization precession with frequencies that are much larger in antiferromagnets than in ferromagnets. This fast magnetization dynamics constitutes one of the motivations for pushing research in antiferromagnetic spintronics.[9–14]

Equation (16) shows that the frequency of the β-mode decreases with an increasing field and vanishes for $H_0 = H_c$, the field value that defines the limit of stability of the AF phase. Note that this value is larger than the one obtained before for the thermodynamic transition, but for small anisotropy, the two expressions are approximately the same $H_{SF} \approx H_c \approx (2H_E H_A)^{1/2}$. With no applied field, the AFMR frequency is $\omega_0 = \gamma H_c$. Using for MnF_2 $g = 2$, $\gamma = 2.8$ GHz/kOe, and $H_c = 93$ kOe, this gives for the AFMR frequency 260 GHz. Using for FeF_2 $g = 2.25$ and $H_c = 505$ kOe, we obtain 1.59 THz.

The AFMR frequencies have been measured in MnF_2 and FeF_2 with several techniques. The first measurements in MnF_2, made in zero field by Johnson and Nethercot[48] with a millimeter microwave spectrometer, showed very broad lineshapes, but served to give the temperature dependence of the AFMR frequency. By applying a large magnetic field along the c axis, Jaccarino and coauthors managed to carry out AFMR experiments in MnF_2 at microwave frequencies to measure the absorption lineshapes and obtain information about the damping mechanisms.[49,50] This technique was also used in Ref. 22 to measure the limit of stability of the AF phase in MnF_2. As shown in Fig. 4(a), measurement of the AFMR frequency vs field and extrapolation to zero-frequency yields a precise value for the field $H_c(T)$.

The complete picture of the field dependence of the two AFMR frequencies in MnF_2 at low temperatures was measured in Ref. 51 using a combination of microwave millimeter and submillimeter sources. Figure 3(b) shows the data of Ref. 51 and the results of the calculations described here for the three phases of spin arrangement in MnF_2. In the AF phase, according to Eq. (16), as the field increases, the frequency of the mode with counterclockwise precession (α) increases, as in a ferromagnet. On the other hand, the frequency of the clockwise precession mode (β) decreases with an increasing field. As we will show in Sec. IV B, in the spin-flop (SF) phase, the frequency of one mode is zero and the other is $\omega_0 = \gamma(H_0^2 - H_c^2)^{1/2}$, as in the data of Fig. 3(b). Note that if the field is applied perpendicularly to the c axis, the equilibrium positions of the sublattice magnetizations are at some angle with the field, characterizing a canted phase. In this case, the two modes are degenerate and there is no spin-flop transition, as will be shown in Sec. IV C. Figure 4(b) shows a comparison of the phase diagrams for MnF_2 measured by various techniques, as presented in Ref. 23. The AFMR has also been investigated in detail in FeF_2 using a conventional far-infrared monochromator[24] and also with transmission measurements employing the radiation of molecular far-infrared lasers.[52,53]

B. Easy-plane antiferromagnets

In the case of the biaxial, or easy-plane, antiferromagnet, Eqs. (11) and (14) yield for the two AFMR frequencies

$$\omega_{\alpha,\beta}^2 = (A^2 + \gamma^2 H_0^2) - (C^2 + B^2) \pm 2\sqrt{\gamma^2 H_0^2 (A^2 - B^2) + B^2 C^2}. \quad (21)$$

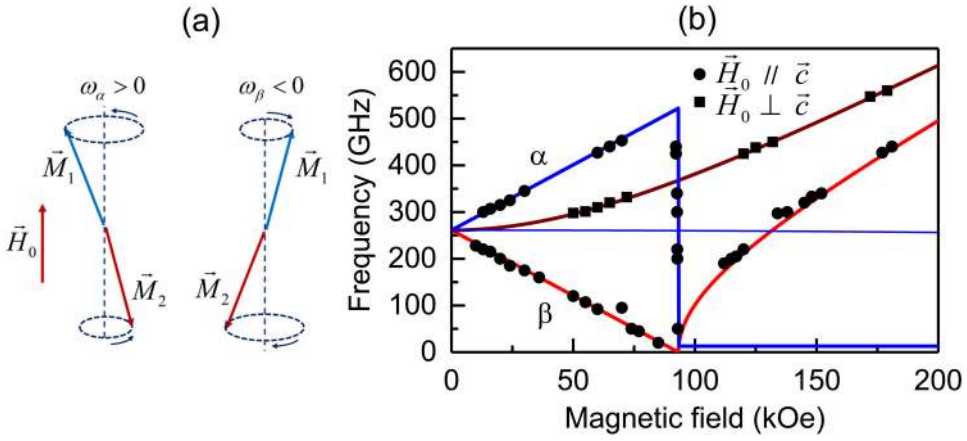

FIG. 3. (a) Illustration of the precessions of the sublattice magnetizations of the two modes of antiferromagnetic resonance in an easy-axis antiferromagnet. (b) Symbols represent the measured magnetic field dependence of the AFMR frequencies in MnF_2 at 1.8–5.0 K, with the field applied parallel and perpendicular to the c-axis.[51] The solid lines represent the field dependencies of the frequencies calculated with Eqs. (16) and (17) for the AF phase, with Eqs. (61) for the SF phase, and with Eqs. (59) and (67) for the canted phase ($\vec{H}_0 \perp \vec{c}$).

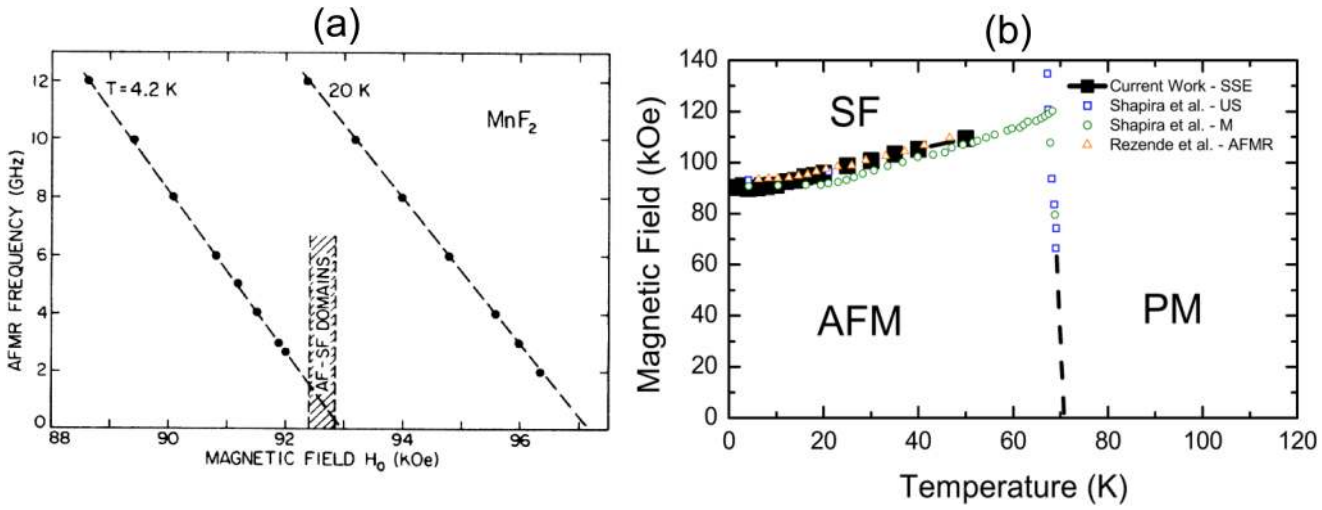

FIG. 4. Experimental data for MnF_2. (a) Measurements of the AFMR frequency vs applied field at two temperature values.[22] Reprinted with permission from S. M. Rezende *et al.*, Phys. Rev. B **16**, 1126 (1977). Copyright 1977 American Physical Society. (b) Phase diagram for MnF_2 measured with various techniques: ultrasonic attenuation (US);[21] differential magnetization (M);[21] antiferromagnetic resonance (AFMR);[22] and spin Seebeck effect (SSE).[23] Reprinted with permission from S. M. Wu *et al.*, Phys. Rev. Lett. **116**, 097204 (2016). Copyright 2016 American Physical Society.

Using the definition of the parameters in Eqs. (12), for $H_E \gg H_{Ax}, H_{Az}$, we have

$$\omega_{\alpha,\beta}^2 \cong \gamma^2\{H_E(H_{Ax}+2H_{Az})+H_0^2 \pm [4H_0^2H_E(H_{Ax}+2H_{Az})+H_E^2H_{Ax}^2]^{1/2}\}. \quad (22)$$

Considering $H_{Ax} \gg H_{Az}$, appropriate for NiO, the two frequencies become simply

$$\omega_{\alpha 0}^2 \approx \gamma^2(2H_EH_{Ax}+3H_0^2), \quad \omega_{\beta 0}^2 \approx \gamma^2(2H_EH_{Az}-H_0^2). \quad (23)$$

On the other hand, for $H_0 = 0$, regardless of the relative values of the anisotropy fields, Eq. (22) gives

$$\omega_{\alpha 0}^2 = \gamma^2 2H_E(H_{Az}+H_{Ax}), \quad \omega_{\beta 0}^2 = \gamma^2 2H_EH_{Az}. \quad (24)$$

Clearly, in the absence of the hard-axis anisotropy, in zero field, the two modes are degenerate, as seen earlier for the uniaxial AF. The presence of the hard-axis anisotropy lifts the degeneracy of the two modes. This feature gives NiO the property of transporting a magnonic spin current even with no applied field.[54] Equations (23) show that as the field increases, the frequency of the α-mode increases, while the one for the β-mode decreases. The β-mode frequency goes to zero at a field $H_{SF} \approx (2H_EH_{Az})^{1/2}$, which represents the limit of stability of the AF phase. Using the values of the effective fields for NiO, $H_E = 9\,684$ kOe, $H_{Ax} = 6.35$ kOe, $H_{Az} = 0.11$ kOe, and $g = 2.18$, we find for the zero-field frequencies approximately 1.07 THz and 0.140 THz. The AFMR of the higher frequency mode, called optical mode, has been measured with several techniques.[34,36]

In order to obtain the eigenstates of the two uniform magnon modes in the AF phase of easy-plane antiferromagnets, we consider $H_0 = 0$ and use for the eigenvalues (frequencies) $\omega_1 = -\omega_2 = \omega_\alpha$ and $-\omega_3 = \omega_4 = \omega_\beta$, given by Eq. (21). The solution of the eigenvalue Eq. (13) gives for the eigenvector matrix

$$[S] = \begin{pmatrix} -\varepsilon_\alpha & \varepsilon_\alpha & \varepsilon_\beta & -\varepsilon_\beta \\ \varepsilon_\alpha & -\varepsilon_\alpha & \varepsilon_\beta & -\varepsilon_\beta \\ 1 & 1 & -1 & -1 \\ 1 & 1 & 1 & 1 \end{pmatrix}, \quad (25)$$

where

$$\varepsilon_\alpha = \frac{\omega_\alpha}{A-(B-C)}, \quad \varepsilon_\beta = \frac{\omega_\beta}{A+(B+C)}, \quad (26)$$

are the ellipticities, defined as $\varepsilon = m_x/i\,m_y$. Using Eqs. (12) and (24), and considering $H_E \gg H_{Ax} \gg H_{Az}$, appropriate for NiO, Eqs. (26) give for the ellipticities

$$\varepsilon_\alpha \approx \left(\frac{2H_E}{H_{Ax}}\right)^{1/2}, \quad \varepsilon_\beta \approx \left(\frac{H_{Az}}{2H_E}\right)^{1/2}. \quad (27)$$

Using the parameters for NiO, Eqs. (27) give for the ellipticities $\varepsilon_\alpha \approx 55$ and $\varepsilon_\beta \approx 1/419$. From Eqs. (25) and (27), we see that in the α-mode $\vec{M}_1$ precesses counterclockwise about the z axis, while $\vec{M}_2$ precesses clockwise, with very elliptical trajectories, with the major axis oriented along the x axis (hard anisotropy axis). The precessions in opposite directions give rise to an oscillating magnetization component in the y-direction, illustrated in Fig. 5. On the other hand, in the β-mode, $\vec{M}_1$ precesses clockwise about the z

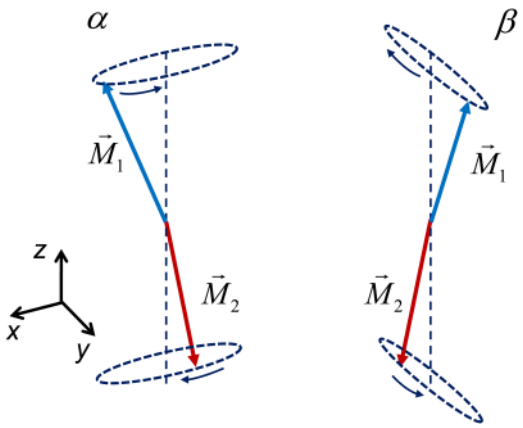

FIG. 5. Illustration of the precessions of the sublattice magnetizations of the two modes of antiferromagnetic resonance in an easy-plane (or hard-axis) antiferromagnet.

axis, while $\vec{M}_2$ precesses counterclockwise, with very elliptical trajectories, with the major axis oriented along the y axis, giving rise to an oscillating magnetization component in the x-direction, as in Fig 5. In Sec. IV D, we shall return to the discussion of the eigenmodes in easy-plane AFs in connection with the spin waves in these materials.

IV. ANTIFERROMAGNETIC MAGNONS

In this section, we present a quantum formulation of spin waves in antiferromagnets. We treat the quantized excitations of the magnetic system with the approach of Holstein–Primakoff (HP),[55] which consists of transformations expressing the spin operators in terms of boson operators that create or annihilate quanta of spin waves, or magnons. This approach was developed for ferromagnets, but it also works well for antiferromagnets.[56] We treat separately the cases of the easy-axis AFs, such as MnF_2 and FeF_2, and that of the easy-plane AF, such as NiO and MnO.

A. Easy-axis antiferromagnets: AF phase

Here we consider that the spins of the two sublattices point in the direction $\pm z$ of the symmetry axis, as in Fig. 1(b), and write the Hamiltonian (1) for the easy-axis AF in terms of raising and lowering spin operators

$$\mathrm{H} = -\gamma\hbar\sum_{i,j}\vec{H}_0\cdot\vec{S}_{i,j} + \sum_{i\neq j}J_{ij}(S_i^+S_j^- + S_i^-S_j^+ + 2S_i^zS_j^z) - D\sum_{i,j}(S_{i,j}^z)^2, \tag{28}$$

where the subscripts i and j refer to the sites in sublattices 1 and 2, respectively. In the first HP transformation, the components of the local spin operators are related to the creation and annihilation operators of spin deviations. For the up-spin sublattice, the lowering spin operator is related to the operator $a_i^\dagger$ that creates a spin deviation, while the raising spin operator is related to the operator a_i that destroys a spin deviation[18,56,57]

$$S_{1i}^+ = (2S)^{1/2}\left(1 - \frac{a_i^\dagger a_i}{2S}\right)^{1/2} a_i, \tag{29a}$$

$$S_{1i}^- = (2S)^{1/2}\, a_i^\dagger\left(1 - \frac{a_i^\dagger a_i}{2S}\right)^{1/2}, \tag{29b}$$

$$S_{1i}^z = S - a_i^\dagger a_i. \tag{29c}$$

For the down-spin sublattice, the raising spin operator is related to the operator that creates a spin deviation, and we have

$$S_{2j}^+ = (2S)^{1/2} b_j^\dagger\left(1 - \frac{b_j^\dagger b_j}{2S}\right)^{1/2}, \tag{30a}$$

$$S_{2j}^- = (2S)^{1/2}\left(1 - \frac{b_j^\dagger b_j}{2S}\right)^{1/2} b_j, \tag{30b}$$

$$S_{2j}^z = -S + b_j^\dagger b_j, \tag{30c}$$

where $a_i^\dagger$, a_i, and $b_j^\dagger$, b_j, are the creation and destruction operators for spin deviations at sites i,j of sublattices 1 and 2, which satisfy the boson commutation rules $[a_i, a_{i'}^\dagger] = \delta_{ii'}$, $[a_i, a_{i'}] = 0$, $[b_j, b_{j'}^\dagger] = \delta_{jj'}$ and $[b_j, b_{j'}] = 0$. The next step consists of introducing a transformation from the localized field operators to collective boson operators that satisfy the commutation rules, $[a_k, a_{k'}^\dagger] = \delta_{kk'}$, $[a_k, a_{k'}] = 0$, $[b_k, b_{k'}^\dagger] = \delta_{kk'}$, $[b_k, b_{k'}] = 0$,

$$a_i = N^{-1/2}\sum_k e^{i\vec{k}.\vec{r}_i}\, a_k, \quad b_j = N^{-1/2}\sum_k e^{i\vec{k}.\vec{r}_j}\, b_k, \tag{31}$$

where N is the number of spins in each sublattice and $\vec{k}$ is a wave vector, and we have the orthonormality condition

$$N^{-1}\sum_i e^{i(\vec{k}-\vec{k}').\vec{r}_i} = \delta_{k,k'}. \tag{32}$$

Introducing in Eq. (28) the transformations (29) and (30) with the binomial expansions of the square roots, and using Eqs. (31) and (32), we obtain a Hamiltonian with the form $\mathrm{H} = E_0 + \mathrm{H}^{(2)} + \mathrm{H}^{(4)} + \mathrm{H}^{(6)} + \cdots$, where each term contains an even number of boson operators. The quadratic part of the Hamiltonian is

$$\mathrm{H}^{(2)} = \gamma\hbar\sum_k (H_E + H_A + H_0)a_k^\dagger a_k + (H_E + H_A - H_0)b_k^\dagger b_k + \gamma_k H_E(a_k b_{-k} + a_k^\dagger b_{-k}^\dagger), \tag{33}$$

where γ_k is a structure factor defined by $\gamma_k = (1/z)\sum_\delta \exp(i\vec{k}\cdot\vec{\delta})$, $\vec{\delta}$ are the vectors connecting the z nearest neighbors in opposite sublattices, and we have considered only intersublattice exchange with

the effective fields defined as in Eq. (3). The next step consists of performing canonical transformations from the collective boson operators $a_k^\dagger$, a_k, $b_k^\dagger$, b_k into magnon creation and annihilation operators $\alpha_k^\dagger$, α_k, $\beta_k^\dagger$, β_k. This is done with the Bogoliubov transformation[18]

$$a_k = u_k\alpha_k - v_k\beta_{-k}^\dagger, \tag{34a}$$

$$b_{-k}^\dagger = -v_k\alpha_k + u_k\beta_{-k}^\dagger. \tag{34b}$$

Substituting these expressions in Eq. (33) and imposing that the Hamiltonian be cast in the diagonal form

$$\mathrm{H}^{(2)} = \sum_k \hbar(\omega_{\alpha k}\,\alpha_k^\dagger\alpha_k + \omega_{\beta k}\,\beta_k^\dagger\beta_k), \tag{35}$$

where ω_{α_k} and ω_{β_k} are the frequencies of the two magnon modes, one can find the frequencies and the transformation coefficients. These are given by

$$\omega_{\alpha_k} = \omega_k + \gamma H_0, \quad \omega_{\beta_k} = \omega_k - \gamma H_0, \tag{36a}$$

$$\omega_k = \gamma[2H_EH_A + H_A^2 + H_E^2(1-\gamma_k^2)]^{1/2} \tag{36b}$$

and

$$u_k = \left(\frac{\gamma H_E + \gamma H_A + \omega_k}{2\omega_k}\right)^{1/2}, \tag{37a}$$

$$v_k = \left(\frac{\gamma H_E + \gamma H_A - \omega_k}{2\omega_k}\right)^{1/2}. \tag{37b}$$

Notice that the transformation coefficients satisfy the orthonormality condition $u_k^2 - v_k^2 = 1$. Using for the body-centered tetragonal structure of MnF_2 and FeF_2, the vectors connecting nearest neighbors $\vec{\delta} = \pm\hat{x}(a/2) \pm \hat{y}(a/2) \pm \hat{z}(c/2)$, one can show that the geometric structure factor is

$$\gamma_k = \cos(k_xa/2)\cos(k_ya/2)\cos(k_zc/2). \tag{38}$$

Note that for magnons with $k = 0$, $\gamma_k = 1$, and Eqs. (36) are the same as Eq. (16) for the AFMR frequencies. Figure 6 shows the magnon dispersion relations for MnF_2, with no applied field, with the wave vector along the c axis, measured by inelastic neutron scattering at three temperatures.[58] The curves in Fig. 6 were calculated with Eqs. (36) and (38) and with the magnon energy renormalization, to be described next, using $H_E = 570$ kOe, $H_A = 8.2$ kOe, and $g = 2.0$. The value of the exchange field was adjusted to fit the data at $T = 3$ K and is about 7% higher than the value given before, because Eq. (36) does not include the effect of the intrasublattice interaction J_1 (see Fig. 1).

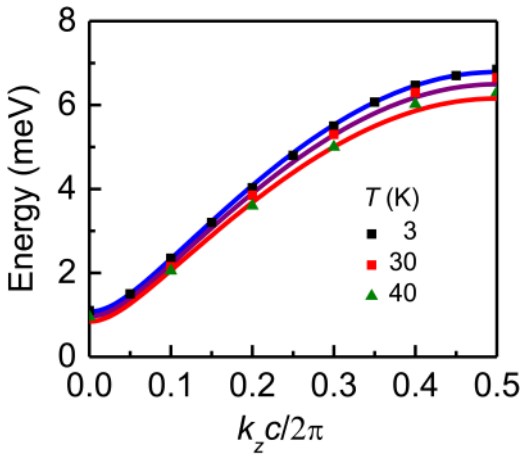

FIG. 6. Magnon dispersion relations for MnF_2 with no applied field with the wave vector along the c-axis. Symbols represent inelastic neutron scattering data at three temperatures,[58] and the solid lines represent the dispersions calculated for the same temperatures with Eqs. (36) and (38) and with the magnon energy renormalization in Eqs. (40) and (41).

The decrease in frequency with increasing temperature is due to the magnon energy renormalization. This was calculated using the terms of the Hamiltonian with four magnon operators, obtained by substitution of the transformations (29)–(31) and (37) in Eq. (28), and retaining only those that have pairs of creation-annihilation operators for the same mode, in any order, such as $\alpha_{k1}\alpha_{k2}^\dagger\alpha_{k3}^\dagger\alpha_{k4}$, $\alpha_{k1}\alpha_{k2}^\dagger\beta_{k3}^\dagger\beta_{k4}$, and $\beta_{k1}\beta_{k2}^\dagger\beta_{k3}^\dagger\beta_{k4}$. Then, we use a random-phase approximation[57] to replace one of the pairs by its thermal average such that the term has the same form as in Eq. (35). For example, $\alpha_{k1}\alpha_{k2}^\dagger\beta_{k3}^\dagger\beta_{k4}\Delta(\vec{k}_1 + \vec{k}_4 - \vec{k}_2 - \vec{k}_3)$ is replaced by $\langle\alpha_q\alpha_q^\dagger\rangle\beta_k^\dagger\beta_k = (\bar{n}_{\alpha q} + 1)\beta_k^\dagger\beta_k + \bar{n}_{\beta q}\alpha_k^\dagger\alpha_k$, where $\bar{n}_{\alpha q,\beta q}$ is the thermal occupation number for the α- or β-mode with wave vector $\vec{q}$, given by the Bose–Einstein distribution $\bar{n}_{\alpha q,\beta q} = 1/(e^{\hbar\omega_{\alpha q,\beta q}/k_BT} - 1)$. The averages of other pairs of operators such as $\alpha_{k1}\alpha_{k2}\beta_{k3}^\dagger\beta_{k4}$, or $\alpha_{k1}\alpha_{k3}^\dagger\beta_{k2}\beta_{k4}$, vanish or do not contribute to the energy of either mode. Applying this approximation to each four-magnon term, the Hamiltonian reduces to a quadratic form

$$\mathrm{H}^{(4)} \Rightarrow \hbar\sum_k \Delta\omega_{\alpha k}\alpha_k^\dagger\alpha_k + \Delta\omega_{\beta k}\beta_k^\dagger\beta_k, \tag{39}$$

where $\hbar\Delta\omega_{\alpha k}$ and $\hbar\Delta\omega_{\beta k}$ represent the renormalization of the energies of the two modes. Thus, clearly the total magnon energies become temperature dependent, given by $\hbar\omega_{\alpha k,\beta k}(T) = \hbar\omega_{\alpha k,\beta k}(0) + \hbar\Delta\omega_{\alpha k,\beta k}(T)$. Using the contributions from the exchange and anisotropy interactions, the total 4-magnon contribution to the α-mode energy becomes[47,59]

$$\begin{aligned}\hbar\Delta\omega_{\alpha k}(T) = 2zJ\,[&(u_k^2 + v_k^2 - 2u_kv_k\gamma_k)C_q + (u_kv_k\gamma_k - v_k^2)E_q \\ &+ (u_kv_k\gamma_k - u_k^2)F_q] - 4D(u_k^2E_q + v_k^2F_q),\end{aligned} \tag{40}$$

where

$$C_q = \frac{1}{NS}\sum_q u_q v_q \gamma_q (\bar{n}_{\alpha q} + \bar{n}_{\beta q} + 1), \tag{41a}$$

$$E_q = \frac{1}{NS}\sum_q u_q^2 \bar{n}_{\alpha q} + v_q^2 (\bar{n}_{\beta q} + 1), \tag{41b}$$

$$F_q = \frac{1}{NS}\sum_q u_q^2 \bar{n}_{\beta q} + v_q^2 (\bar{n}_{\alpha q} + 1). \tag{41c}$$

The correction for the frequency of the β-mode is given by the same expressions as (40) and (41) with the interchange $\alpha \leftrightarrow \beta$. It is important to note that even at $T = 0$ there is a correction to the magnon energies due to the magnon interactions. This zero-point correction is a characteristic feature of antiferromagnets that was first noted by Oguchi several decades ago.[60]

The temperature dependence of the magnon energy renormalization for MnF_2 due to 4-magnon interactions was calculated numerically with Eqs. (40) and (41) replacing the sum over wave vectors by an integral over the Brillouin zone

$$\frac{1}{N}\sum_k \rightarrow \frac{\Omega}{(2\pi)^3}\int d\vec{k}, \tag{42}$$

where N is the number of allowed $\vec{k}$ values in the first Brillouin zone and Ω is the volume of the unit cell. For each temperature, the integrals in (41) were evaluated numerically by discrete sums in $\vec{k}$ space. In the first cycle of the evaluation of $\Delta\omega_{\alpha k}$ and $\Delta\omega_{\beta k}$, the frequencies and the Bose factors are calculated for each point k in the Brillouin zone without renormalization. In the following cycles, the new Bose factors are calculated with the magnon frequencies $\hbar\omega_{\alpha k,\beta k}(T) = \hbar\omega_{\alpha k,\beta k}(0) + \hbar\Delta\omega_{\alpha k,\beta k}(T)$, using the renormalized energies of the previous cycle. The process is repeated until the change in frequency at all points is smaller than 0.1%. Figure 5 shows that the calculated dispersion relations in MnF_2 for three temperature values agree quite well with the experimental data.

B. Easy-axis antiferromagnets: SF phase

As mentioned earlier, if the applied field H_0 exceeds the critical value H_c, the energy of the β-mode at $k = 0$, given by Eq. (16), becomes negative and the AF phase is no longer stable. Then the spins flip to the configuration illustrated in Fig. 1(b), at an angle $\theta_1 = \theta_2 = \theta$ with the field and in a plane determined by the small anisotropy that exists in the plane normal to the symmetry axis. We shall study the spin wave excitations in the SF phase using two different coordinate systems, one for each sublattice, as shown in Fig. 7. In each system, the z axis is chosen to point along the spin equilibrium direction in that sublattice, the y-axes are in the direction of the y axis of the crystal, as in Fig. 1, and the x-axes are determined by $\hat{x} = \hat{y} \times \hat{z}$.

As in Sec. IV A, we express the spin components in each sublattice in terms of spin deviation operators. Considering only the first order terms in the binomial expansions of the square roots in

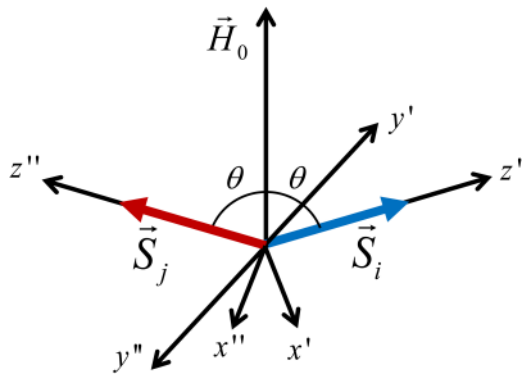

FIG. 7. Coordinate systems used to represent the components of the spin operators for the two sublattices in the spin flop phase.

Eqs. (29), we have

$$S_i^+ = S_i^{x'} + iS_i^{y'} = \sqrt{2S}\, a_i, \quad S_j^+ = S_j^{x''} + iS_j^{y''} = \sqrt{2S}\, b_j, \tag{43a}$$

$$S_i^- = S_i^{x'} - iS_i^{y'} = \sqrt{2S}\, a_i^\dagger, \quad S_j^- = S_j^{x''} - iS_j^{y''} = \sqrt{2S}\, b_j^\dagger, \tag{43b}$$

$$S_i^{z'} = S - a_i^\dagger a_i, \quad S_j^{z''} = S - b_j^\dagger b_j. \tag{43c}$$

Using the transformation to collective boson operators in Eq. (31) and the relation (32), one can show that the Hamiltonian (28) leads to the following quadratic form:

$$\mathrm{H}^{(2)} = \hbar\sum_k A_k(a_k^\dagger a_k + b_k^\dagger b_k) + B_k(a_k b_{-k} + a_k^\dagger b_{-k}^\dagger) + \frac{1}{2}C_k(a_k a_{-k} + b_k b_{-k} + H.c.) + D_k(a_k b_k^\dagger + a_k^\dagger b_k), \tag{44}$$

where

$$A_k = \gamma\left[H_0\cos\theta - H_E\cos 2\theta + H_A\left(\cos^2\theta - \frac{1}{2}\sin^2\theta\right)\right], \tag{45a}$$

$$B_k = \gamma\gamma_k H_E \sin^2\theta, \quad C_k = \frac{1}{2}\gamma H_A \sin^2\theta, \quad D_k = \gamma\gamma_k H_E \cos^2\theta, \tag{45b}$$

where the angle is given $\theta = \cos^{-1}[H_0/(2H_E - H_A)]$. The next step consists of performing canonical transformations from the collective boson operators $a_k^\dagger$, a_k, $b_k^\dagger$, b_k into magnon creation and annihilation operators $\alpha_k^\dagger$, α_k, $\beta_k^\dagger$, β_k such that the quadratic Hamiltonian is cast in the diagonal form (35).

Here, we follow the method developed by White *et al.*[61] that generalizes the Bogoliubov transformation for diagonalizing

quadratic Hamiltonians and write Eq. (44) in the matrix form

$$\mathrm{H} = \hbar \sum_{k>0} \mathrm{H}_k, \quad \mathrm{H}_k = (X)^\dagger [\mathrm{H}](X), \tag{46}$$

where the matrices are

$$(X) = \begin{pmatrix} a_k \\ b_k \\ a^\dagger_{-k} \\ b^\dagger_{-k} \end{pmatrix}, \quad [\mathrm{H}] = \hbar \begin{pmatrix} A_k & D_k & C_k & B_k \\ D_k & A_k & B_k & C_k \\ C_k & B_k & A_k & D_k \\ B_k & C_k & D_k & A_k \end{pmatrix}. \tag{47}$$

The next step consists of introducing a linear transformation to new operators

$$(X) = [Q](Z), \quad (Z) = \begin{pmatrix} \alpha_k \\ \beta_k \\ \alpha^\dagger_{-k} \\ \beta^\dagger_{-k} \end{pmatrix} \tag{48}$$

such that the Hamiltonian in Eq. (46) can be written as

$$\mathrm{H} = \hbar \sum_k (Z)^\dagger [\omega](Z), \tag{49}$$

where $[\omega]$ is a diagonal eigenvalue matrix. In order to find the transformation matrix $[Q]$, one needs a few relations. The first follows from the introduction of (48) in (46) and comparison with (49). This leads to

$$[Q]^\dagger [\mathrm{H}][Q] = \hbar[\omega]. \tag{50}$$

Another relation is obtained from the boson commutation rules. They can be written in matrix form as

$$[X, X^\dagger] = X(X)^\dagger - (X^* X^T)^T = [g], \tag{51a}$$

$$[Z, Z^\dagger] = Z(Z)^\dagger - (Z^* Z^T)^T = [g], \tag{51b}$$

where

$$[\mathrm{g}] = \begin{bmatrix} 1 & 0 & 0 & 0 \\ 0 & 1 & 0 & 0 \\ 0 & 0 & -1 & 0 \\ 0 & 0 & 0 & -1 \end{bmatrix}. \tag{52}$$

Using Eqs. (47) and (48) in (51a) and in (51b), we obtain an orthonormality relation for the transformation matrix

$$[Q][g][Q]^\dagger = [g], \tag{53}$$

and with (50)–(52) we obtain the eigenvalue equation

$$[\mathrm{H}][Q] = [g]^{-1}[Q][g]\hbar[\omega]. \tag{54}$$

The solution of this equation gives the eigenfrequencies and the elements of the transformation matrix $[Q]$. Due to the symmetry of the 4×4 matrices, the matrix equations can be reduced to relations between 2×2 matrices. This is done by first noticing that the Hamiltonian (47) can be written as

$$[\mathrm{H}] = \begin{bmatrix} [H_1] & [H_2] \\ [H_2] & [H_1] \end{bmatrix}, \quad [\mathrm{H}_1] = \hbar \begin{bmatrix} A_k & D_k \\ D_k & A_k \end{bmatrix}, \quad [\mathrm{H}_2] = \hbar \begin{bmatrix} C_k & B_k \\ B_k & C_k \end{bmatrix}. \tag{55}$$

Also, note that the transformations of the operators a_k and b_k are the complex conjugates of the ones for $a^\dagger_{-k}$ and $b^\dagger_{-k}$ so that the matrix $[Q]$ can also be written in terms of submatrices

$$[Q] = \begin{bmatrix} [Q_1] & [Q_2] \\ [Q_2^*] & [Q_1^*] \end{bmatrix}, \quad [Q_1] = \begin{bmatrix} Q_{11} & Q_{12} \\ Q_{21} & Q_{22} \end{bmatrix}, \quad [Q_2] = \begin{bmatrix} Q_{13} & Q_{14} \\ Q_{23} & Q_{24} \end{bmatrix}. \tag{56}$$

The matrix $[g]$ in (52) can also be written in the form

$$[g] = \begin{bmatrix} I & 0 \\ 0 & -I \end{bmatrix}, \tag{57}$$

where I is a 2×2 diagonal unit matrix. Using Eqs. (55)–(57) in (47), we obtain the following relations between the 2×2 matrices

$$[H_1][Q_1] + [H_2][Q_2^*] = \hbar\,[Q_1][\omega], \tag{58a}$$

$$[H_1][Q_2] + [H_2][Q_1^*] = -\hbar[Q_2][\omega]. \tag{58b}$$

The solution of Eqs. (58) yields the diagonal Hamiltonian in Eq. (35), with the eigenfrequencies given by

$$\omega^2_{\alpha k} = (A_k - D_k)^2 - (B_k - C_k)^2, \tag{59a}$$

$$\omega^2_{\beta k} = (A_k + D_k)^2 - (B_k + C_k)^2 \tag{59b}$$

and the elements of the transformation matrix given by

$$Q_{11} = \left[\frac{(A_k - D_k) + \omega_{\alpha k}}{4\omega_{\alpha k}}\right]^{1/2}, \quad Q_{12} = -\left[\frac{(A_k + D_k) + \omega_{\beta k})}{4\omega_{\beta k}}\right]^{1/2}, \tag{60a}$$

$$Q_{13} = \left[\frac{(A_k - D_k) - \omega_{\alpha k}}{4\omega_{\alpha k}}\right]^{1/2}, \quad Q_{14} = \left[\frac{(A_k + D_k) - \omega_{\beta k})}{4\omega_{\beta k}}\right]^{1/2}, \tag{60b}$$

and $Q_{21} = -Q_{11}$, $Q_{22} = Q_{12}$, $Q_{23} = -Q_{13}$, $Q_{24} = Q_{14}$. These results greatly simplify if H_0, $H_A \ll H_E$, which is the case of MnF_2. Using

for $ka \ll 1$, $1-\gamma_k \approx (ka)^2/8$, the two magnon frequencies become

$$\omega_{\alpha k} \approx \frac{1}{2}\gamma H_E\, a\, k, \tag{61a}$$

$$\omega_{\beta k} \approx \gamma\left(H_0^2 - H_c^2 + \frac{1}{4}H_E^2\, a^2 k^2\right)^{1/2}. \tag{61b}$$

As we saw in Sec. IV B, in the AF phase, the frequency of the α_k mode increases linearly with magnetic field intensity for any wave vector. However, in the SF phase, the frequency becomes independent of the applied field and, moreover, it vanishes for the $k=0$ magnon, as can be seen in Eq. (61a). This behavior has been clearly observed experimentally in MnF_2,[51] as shown in Fig. 3(b). The frequency increases linearly with field, but as the field approaches H_c, it falls abruptly to a very small value. This is so because this mode corresponds to the rotation of the spins about the symmetry axis at no cost of energy. In fact, in crystals there is always a small anisotropy in the plane perpendicular to the symmetry axis that can be represented by an effective field H_{Ap}. In this case, the frequency of the $k=0$, α_k magnon is $\omega_{\alpha 0} = \gamma(2H_E H_{Ap})^{1/2}$, which is still independent of the applied field, but not zero. In regard to the β_k mode, in the AF phase, its frequency decreases linearly with field and, for the $k=0$ magnon, it goes to zero at $H_0 = H_c$. For $H_0 > H_c$, according to Eq. (61b), the frequency increases with field as $\omega_{\beta k} = \gamma(H_0^2 - H_c^2)^{1/2}$, in agreement with the experimental data shown in Fig. 3(b).

We can find the behavior of the sublattice spins of the magnon modes in the SF phase, by calculating the expectation values of the spin components in coherent magnon states.[62,63] For the α_k mode, we obtain

$$\langle S_i^{x'}\rangle = (2S/N)^{1/2}(Q_{11}+Q_{13})|\alpha_k|\cos(\vec{k}\cdot\vec{r}_i - \omega_{\alpha k} + \phi_{\alpha k}), \tag{62a}$$

$$\langle S_i^{y'}\rangle = (2S/N)^{1/2}(Q_{11}-Q_{13})|\alpha_k|\sin(\vec{k}\cdot\vec{r}_i - \omega_{\alpha k} + \phi_{\alpha k}), \tag{62b}$$

$$\langle S_j^{x''}\rangle = -(2S/N)^{1/2}(Q_{11}+Q_{13})|\alpha_k|\cos(\vec{k}\cdot\vec{r}_j - \omega_{\alpha k} + \phi_{\alpha k}), \tag{62c}$$

$$\langle S_j^{y''}\rangle = -(2S/N)^{1/2}(Q_{11}-Q_{13})|\alpha_k|\sin(\vec{k}\cdot\vec{r}_j - \omega_{\alpha k} + \phi_{\alpha k}), \tag{62d}$$

where $\alpha_k = |\alpha_k|\exp(i\phi_{\alpha k})$. For the β_k mode, we have

$$\langle S_i^{x'}\rangle = (2S/N)^{1/2}(Q_{14}+Q_{12})|\beta_k|\cos(\vec{k}\cdot\vec{r}_i - \omega_{\beta k} + \phi_{\beta k}), \tag{63a}$$

$$\langle S_i^{y'}\rangle = (2S/N)^{1/2}(Q_{14}-Q_{12})|\beta_k|\sin(\vec{k}\cdot\vec{r}_i - \omega_{\beta k} + \phi_{\beta k}), \tag{63b}$$

$$\langle S_j^{x''}\rangle = (2S/N)^{1/2}(Q_{14}+Q_{12})|\beta_k|\cos(\vec{k}\cdot\vec{r}_j - \omega_{\beta k} + \phi_{\beta k}), \tag{63c}$$

$$\langle S_j^{y''}\rangle = (2S/N)^{1/2}(Q_{14}-Q_{12})|\beta_k|\sin(\vec{k}\cdot\vec{r}_j - \omega_{\beta k} + \phi_{\beta k}), \tag{63d}$$

where $\beta_k = |\beta_k|\exp(i\phi_{\beta k})$. With Eqs. (62) and (63), we can find the ellipticities of the spin precessions. Considering $H_E \gg H_0, H_A$ in the coefficients (60), the ellipticity in both sublattices for the α_k mode is

$$e_\alpha = \frac{\langle S_i^{x'}\rangle_{\max}}{\langle S_i^{y'}\rangle_{\max}} = \frac{Q_{11}+Q_{13}}{Q_{11}-Q_{13}} \approx \frac{(\gamma H_E+\omega_{\alpha k})^{1/2} + (\gamma H_E - \omega_{\alpha k})^{1/2}}{(\gamma H_E+\omega_{\alpha k})^{1/2} - (\gamma H_E - \omega_{\alpha k})^{1/2}}, \tag{64}$$

and similarly for the β_k mode, it is

$$e_\beta = \frac{\langle S_i^{x'}\rangle_{\max}}{\langle S_i^{y'}\rangle_{\max}} = \frac{Q_{14}+Q_{12}}{Q_{14}-Q_{12}} \approx \frac{(\gamma H_E+\omega_{\beta k})^{1/2} - (\gamma H_E - \omega_{\beta k})^{1/2}}{(\gamma H_E+\omega_{\beta k})^{1/2} + (\gamma H_E - \omega_{\beta k})^{1/2}}. \tag{65}$$

These equations show that the ellipticity of the spin precession varies strongly with the wave number. Near the center of the Brillouin zone, Eqs. (61) show that the frequencies are $\omega_{\alpha k}, \omega_{\beta k} \ll \gamma H_E$ so that the ellipticities become $e_\alpha = 8\gamma H_E/\omega_{\alpha k}$ and $e_\beta = \omega_{\beta k}/(8\gamma H_E)$. In this case, the spin precessions are highly elliptical, with the major axis much larger than the minor. Figure 8 illustrates the precessions of the spins in the two sublattices for both modes, with $k=0$. In the field-independent α_k mode, the spins precess with the major axes along the x-axes of the two sublattices, with a net spin component along the external field. Thus, this mode can be driven by a *rf* field parallel to the static field. On the other hand, in the field dependent β_k mode, the major axes of the elliptical precessions are along the y-direction for each sublattice, with a

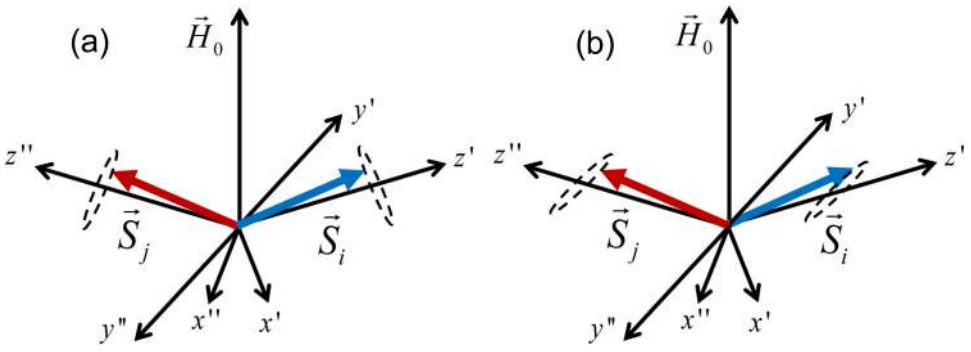

FIG. 8. Illustration of the elliptical precessions of the sublattice spins in the $k=0$ magnon modes in the spin-flop phase. (a) α_k mode. (b) β_k mode.

net spin component along y so that it can be driven by a *rf* field parallel to this direction. However, for magnons at the Brillouin zone boundaries, $\omega_{\alpha k} \approx \omega_{\beta k} \approx \gamma H_E$, and Eqs. (64) and (65) show that $e_\alpha \approx e_\beta \approx 1$ so that the spin precessions are circular.

C. Easy-axis antiferromagnets: Canted phase

We now consider the configuration where the external magnetic field is applied in a direction perpendicular to the easy axis, the c axis in MnF_2 and FeF_2. In this case, in the equilibrium configuration, the two sublattice spins lie in the same plane along directions at an angle θ with the field, similar to the spin-flop phase, shown in Fig. 1(b). Minimization of the energy gives $\cos\theta = H_0/(2H_E + H_A)$. In this phase, the Hamiltonian (28) expressed in terms of boson operators introduced by the transformations in Eqs. (43) and (31) becomes, with only the quadratic terms

$$\mathrm{H} = \hbar \sum_k A_k(a_k^\dagger a_k + b_k^\dagger b_k) + B_k(a_k b_{-k} + a_k^\dagger b_{-k}^\dagger) + \frac{1}{2} C_k(a_k a_{-k} + b_k b_{-k} + H.c.) + D_k(a_k b_k^\dagger + a_k^\dagger b_k), \quad (66)$$

where

$$A_k = \gamma\,[H_0 \cos\theta - H_E \cos 2\theta + H_A(2\sin^2\theta - \cos^2\theta)/2], \quad (67a)$$

$$B_k = \gamma\,\gamma_k H_E \sin^2\theta, \quad (67b)$$

$$C_k = \gamma\,H_A \cos^2\theta/2, \quad (67c)$$

$$D_k = \gamma\,\gamma_k H_E(1 + \cos 2\theta)/2. \quad (67d)$$

The Hamiltonian (66) has the same form as Eq. (44) for the spin-flop state so that the frequencies and the transformation coefficients are given by the same expressions as in Eqs. (59) and (60), with the parameters defined by Eqs. (67).

Figure 9(a) shows the magnon dispersion relations for MnF_2 with a magnetic field of $H_0 = 200$ kOe applied perpendicularly to the easy axis, calculated with Eqs. (59) and (67), using $H_E = 570$ kOe, $H_A = 8.2$ kOe, $g = 2.0$, and a geometric structure factor for a spherical Brillouin zone, $\gamma_k = \cos(\pi k/2k_{\max})$. For the zero field, the two modes are degenerate and the dispersion relations are the same as in Fig. 6. Application of the field results in a behavior similar to the spin-flop phase, the frequency of the α-mode becomes independent of the field, while the frequency of the β-mode increases with the field. This is illustrated further in Fig. 9(b) showing the field dependence of the frequencies for the $k = 0$ modes. The frequency of the β-mode increases continuously with field, as observed experimentally,[51] and shown in Fig. 3(b). Note that the frequency of the α-mode is not shown in Fig. 3(b) because the experiments of Ref. 51 were carried out with fixed frequency and scanning field so that the α-mode could not be detected.

D. Easy-plane antiferromagnets in the AF phase

We now consider easy-plane, or hard-axis, antiferromagnets, initially with no applied field. As in the previous cases, the first step consists in writing the Hamiltonian (5), with $H_0 = 0$, in terms of raising and lowering spin operators

$$\mathrm{H} = -\gamma\hbar \sum_{i,j} J_{ij}(S_i^+ S_j^- + S_i^- S_j^+ + 2S_i^z S_j^z) + \sum_{i,j} D_x(S_{i,j}^x)^2 - D_z(S_{i,j}^z)^2. \quad (68)$$

Next, we use Eqs. (29)–(32) for the transformation from the spin operators into boson collective spin deviation operators and obtain the quadratic Hamiltonian

$$\mathrm{H} = \hbar \sum_k A_k(a_k^\dagger a_k + b_k^\dagger b_k) + B_k(a_k b_{-k} + a_k^\dagger b_{-k}^\dagger) + \frac{1}{2} C_k(a_k a_{-k} + b_k b_{-k} + H.c.), \quad (69)$$

where the parameters are related to the effective fields by

$$A_k = \gamma(H_E + H_{Ax}/2 + H_{Az}), \quad B_k = \gamma\,\gamma_k H_E, \quad C_k = \gamma\frac{H_{Ax}}{2}, \quad (70)$$

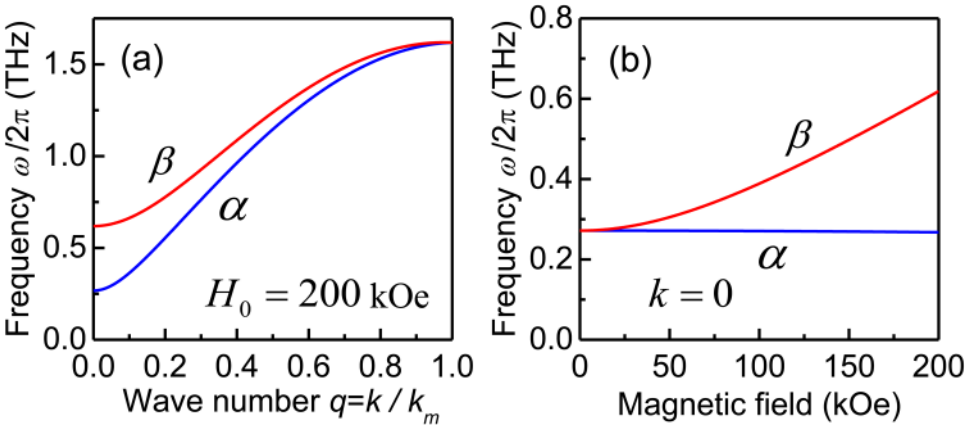

FIG. 9. Magnon frequencies calculated with Eqs. (59) and (67) for MnF_2, with the external field applied perpendicularly to the easy axis, in the spin-canted configuration. (a) Dispersion relations for $H_0 = 200$ kOe. (b) Field dependence of the $k = 0$ magnon frequencies.

where γ_k is the geometric structure factor. The Hamiltonian (69) has the same form as Eq. (44) for the spin flop state so that the frequencies are given by the same expressions as in Eqs. (59a) and (59b), with $D_k = 0$. Thus, the magnon frequencies of the two modes are

$$\omega^2_{\alpha,\beta} = A^2_k - (C_k \mp B_k)^2. \tag{71}$$

Using the expressions for the parameters in Eq. (70), one can write the frequencies of the two magnon modes in terms of the effective fields

$$\omega^2_{\alpha k} = \gamma^2[H^2_{Az} + 2H_E H_{Az} + H_{Ax}H_{Az} + H_E H_{Ax}(1+\gamma_k) + H^2_E(1-\gamma^2_k)], \tag{72a}$$

$$\omega^2_{\beta k} = \gamma^2[H^2_{Az} + 2H_E H_{Az} + H_{Ax}H_{Az} + H_E H_{Ax}(1-\gamma_k) + H^2_E(1-\gamma^2_k)]\,. \tag{72b}$$

For NiO, considering $H_E \gg H_{Ax}, H_{Az}$, the frequencies of the Brillouin-zone center $k = 0$ ($\gamma_k = 1$) magnons are

$$\omega_{\alpha 0} = \gamma[2H_E(H_{Ax} + H_{Az})]^{1/2}, \tag{73a}$$

$$\omega_{\beta 0} = \gamma(2H_E H_{Az})^{1/2}, \tag{73b}$$

which agree with Eq. (24) obtained with the semi-classical treatment. These equations show that, regardless of the relative values of the anisotropy fields, the frequency of the α-mode is always larger than for the β-mode. In the case of NiO, $H_{Ax} \gg H_{Az}$ so that $\omega_{\alpha 0} \approx \gamma(2H_{Ax}H_E)^{1/2}$, in agreement with Eq. (24) for the α-mode and $H_0 = 0$. As shown in Ref. 54, the values of the parameters for NiO can be obtained by fitting Eqs. (72) to three sets of experimental data. Fitting to the neutron scattering measurements of Hutchings and Samuelsen[28] gives the value of the exchange field $H_E = 9\,684$ kOe, considering for the g-factor $g = 2.18$. Since the neutron data do not have sufficient resolution to determine the frequencies of the zone-center magnons, we use the value $\omega_{\beta 0}/2\pi = 0.140$ THz measured by Brillouin light scattering[32] and $\omega_{\alpha 0}/2\pi = 1.07$ THz obtained from magnetization oscillations in the far infrared.[36] With these values in Eqs. (73), we determine the effective anisotropy fields, $H_{Ax} = 6.35$ kOe and $H_{Az} = 0.11$ kOe. Figure 10(a) shows the dispersion relations calculated with Eqs. (72) assuming a spherical Brillouin zone and using for the structure factor $\gamma_k = \cos(\pi k/2k_m)$, where $k_m = \pi/a_l$, a_l being the lattice parameter, as well as the data of Ref. 28. The two magnon modes are nearly degenerate for large wave vectors, but the frequency separation is evident in the blow up near the Brillouin zone center as shown in Fig. 10(b).

In the case where an external field is applied in the easy plane, in a direction along the easy axis, it can be shown[47] that the unrenormalized magnon frequencies are

$$\omega^2_{\alpha,\beta} = (A^2_k + \gamma^2 H^2_0) - (C^2_k + B^2_k) \pm 2\sqrt{\gamma^2 H^2_0(A^2_k - B^2_k) + B^2_k C^2_k}. \tag{74}$$

The dashed lines in Fig. 10(b) represent the dispersion relations in NiO calculated for a field $H_0 = 40$ kOe. As one can see, for $k = 0$, the frequency of the α_k-mode increases with an increasing field, while the frequency of the β_k-mode decreases. In fact, the softening of the β_k-mode with an increasing field determines the spin-flop transition in NiO.[47]

Similar to the case of the spin-flop phase, studied in Sec. IV B, we can calculate the expectation values of the spin components in coherent magnon states in the AF phase of the easy-plane antiferromagnets. In both modes, the spin precessions in the two sublattices are characterized by an ellipticity $e = \langle S^x_{i,j}\rangle_{\max}/\langle S^y_{i,j}\rangle_{\max}$. Using the transformations (30)–(32) and (48), one can express the spin components in terms of the coefficients in Eqs. (60) and show that the ellipticities for modes α_k and β_k are

$$e_\alpha = \frac{Q_{11} + Q_{13}}{Q_{11} - Q_{13}}, \quad e_\beta = \frac{Q_{14} - |Q_{12}|}{Q_{14} + |Q_{12}|}. \tag{75}$$

As in the spin-flop phase, the ellipticities of the spin precession vary strongly with the wave number. Near the center of the

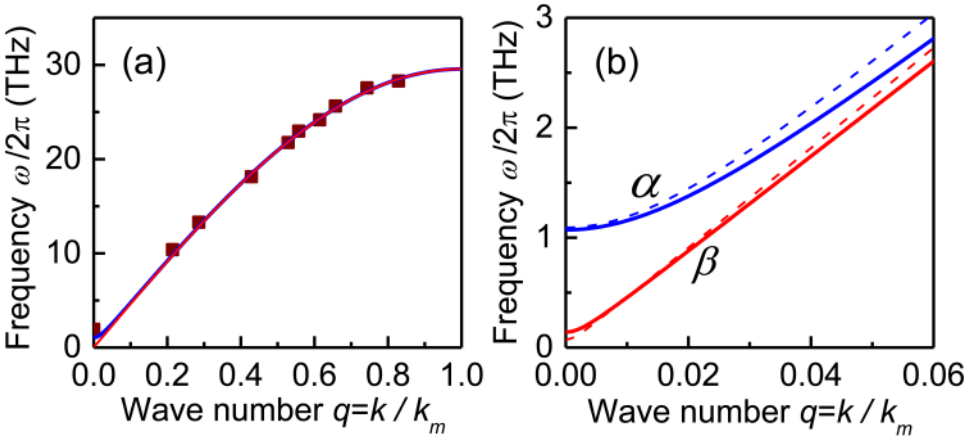

FIG. 10. Spin wave dispersion relations in antiferromagnetic NiO at $T = 300$ K. (a) Solid curves show the magnon frequencies calculated with Eqs. (72). Symbols represent the neutron scattering data of Ref. 28. (b) Blow up of the Brillouin zone center showing the separation of the frequencies of the α (upper blue curve) and β (lower red curve) magnon modes. The dashed curves are calculated with Eq. (74) for a field of $H_0 = 40$ kOe applied along the easy axis.

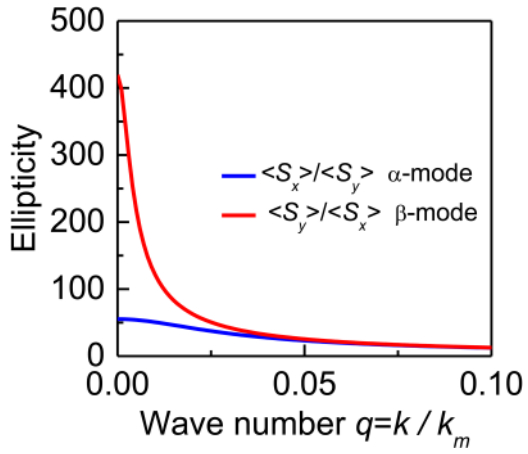

FIG. 11. Wave number dependence of the ellipticities of the two magnon modes in the easy-plane antiferromagnet NiO.

Brillouin zone, for $\gamma H_E \gg \omega_{\alpha k}, \omega_{\beta k}$, Eqs. (75) give the same results as in Eqs. (27), showing that the spin precessions are highly elliptical, as in Fig. 5. However, for magnons near the Brillouin zone boundaries, $\omega_{\alpha k} \approx \omega_{\beta k} \approx \gamma H_E$, Q_{13}, $Q_{14} \to 0$, and one can see from Eq. (75) that the ellipticities approach unity, corresponding to circular spin precessions. The dependencies of the ellipticities on the wave number, calculated for NiO with Eq. (75), are shown in Fig. 11.

V. MAGNONIC SPIN CURRENT IN ANTIFERROMAGNETS

A key concept in spintronics is the spin current, which expresses the flow of spin angular momentum in a material. In metals, the spin current is carried by the spins of the conduction electrons, whereas in magnetic insulators, the spin current is transported by magnons. In a simple ferromagnetic insulator with one spin per unit cell so that there is only one magnon mode, considering z the equilibrium direction of the spins, the spin-current density with polarization z carried by magnons with wave vector $\vec{k}$ and energy $\varepsilon_k = \hbar\omega_k$ is[64–66]

$$\vec{J}_S^z = \frac{\hbar}{(2\pi)^3}\int d^3k\, \vec{v}_k [n_k(\vec{r}) - n_k^0]. \tag{76}$$

Here, $\vec{v}_k$ is the magnon velocity, $n_k(\vec{r})$ is the number of magnons with wave vector $\vec{k}$ at a position $\vec{r}$, and n_k^0 is the number in thermal equilibrium, given by the Bose–Einstein distribution with zero chemical potential. In a two-sublattice antiferromagnet, the spin current is transported by the two magnon modes. In the AF phase, the total z-component of the spin angular momentum carried by magnons is given by $S^z = \sum_{i,j}(S_i^z + S_j^z)$. With Eqs. (29c) and (30c), one can write the z-component of the spin angular momentum as

$$S^z = \sum_k -a_k^\dagger a_k + b_k^\dagger b_k. \tag{77}$$

Using the transformation to the magnon operators given by Eqs. (31) and keeping only terms with magnon number operators, we have

$$S^z = \sum_k (-\alpha_k^\dagger \alpha_k + \beta_k^\dagger \beta_k). \tag{78}$$

The opposite signs in the angular momenta of the two modes are consistent with the semiclassical picture of the spins precessing in opposite directions. Considering for each mode μ the group velocity $\vec{v}_{\mu k} = \hat{k}\,\partial\omega_\mu/\partial k$, the spin current density operator is

$$\vec{J}_S^z = \frac{\hbar}{V}\sum_k [-\vec{v}_{\alpha k}\alpha_k^\dagger \alpha_k + \vec{v}_{\beta k}\beta_k^\dagger \beta_k]. \tag{79}$$

In this equation, which is valid for both easy-axis and hard-axis antiferromagnets, $\alpha_k^\dagger \alpha_k$ and $\beta_k^\dagger \beta_k$ represent the number operators of magnons of each mode. In easy axis antiferromagnets, such as MnF_2 and FeF_2, in the absence of an applied magnetic field, the two magnon modes are degenerate and thus have equal occupation numbers in thermal equilibrium. Since they also have equal group velocities, in easy-axis AFs, the spin current created by thermal gradients vanishes at zero field.

In order to illustrate a method to calculate the magnonic spin current in spintronics, we consider the spin Seebeck effect, which consists of the generation of spin currents by a thermal gradient across a thin layer of a magnetic material.[67–69] In this case, the magnonic spin current can be calculated with the Boltzmann and diffusion equations for the magnon accumulation, defined for AF materials by extending the concept introduced for ferromagnets.[65] Denoting by $n_{\mu k}$ the number of magnons in the $\mu = \alpha, \beta$ mode with wave number k in the whole volume V of the AF layer, and by $n_{\mu k}^0$ the number in thermal equilibrium, given by the Bose–Einstein distribution, the quantity $\delta n_{\mu k}(\vec{r}) = n_{\mu k}(\vec{r}) - n_{\mu k}^0$ is the number in excess of equilibrium. Since the contributions of the two modes to the spin current have opposite signs, we define the magnon accumulation $\delta n_m(\vec{r})$ in antiferromagnets as[54,66,70]

$$\delta n_m(\vec{r}) = \frac{1}{(2\pi)^3}\int d^3k[(n_{\alpha k} - n_{\alpha k}^0) - (n_{\beta k} - n_{\beta k}^0)], \tag{80}$$

so that the magnon spin-current density in Eq. (76) becomes

$$\vec{J}_S^z = -\frac{\hbar}{(2\pi)^3}\int d^3k\,[\vec{v}_{\alpha k}(n_{\alpha k}(\vec{r}) - n_{\alpha k}^0) - \vec{v}_{\beta k}(n_{\beta k}(\vec{r}) - n_{\beta k}^0)]. \tag{81}$$

The distribution of the magnon number under the influence of a thermal gradient can be calculated with the Boltzmann transport equation. In the absence of external forces and in the relaxation approximation, in steady state, we obtain for each magnon mode

$$n_{\mu k}(\vec{r}) - n_{\mu k}^0 = -\tau_{\mu k}\vec{v}_{\mu k}\cdot\nabla n_{\mu k}^0 - \tau_{\mu k}\vec{v}_{\mu k}\cdot\nabla[n_{\mu k}(\vec{r}) - n_{\mu k}^0], \tag{82}$$

where $\tau_{\mu k}$ is the μk-magnon relaxation time. Using Eq. (82) in Eq. (81), one can show that the spin current is the sum of two

parts, $\vec{J}_S^z = \vec{J}_{S\nabla T}^z + \vec{J}_{S\delta n}^z$, where

$$\vec{J}_{S\nabla T}^z = \frac{\hbar}{(2\pi)^3}\int d^3k\left[-\tau_{\alpha k}v_{\alpha ky}^2\frac{\partial n_{\alpha k}^0}{\partial T} + \tau_{\beta k}v_{\beta ky}^2\frac{\partial n_{\beta k}^0}{\partial T}\right]\frac{\partial T}{\partial y} \quad (83)$$

is the contribution of the flow (convection) of magnons due to the temperature gradient, assumed to be in the y direction, and

$$\vec{J}_{S\delta n}^z = -\frac{\hbar}{(2\pi)^3}\int d^3k[\tau_{\alpha k}\vec{v}_{\alpha k}\vec{v}_{\alpha k}\cdot\nabla\delta n_{\alpha k} - \tau_{\beta k}\vec{v}_{\beta k}\vec{v}_{\beta k}\cdot\nabla\delta n_{\beta k}] \quad (84)$$

is due to the spatial variation of the magnon accumulation, which is governed by the diffusion equation.[65,66] With the temperature gradient normal to the film plane, Eq. (83) gives for the spin current in the y-direction[66]

$$J_S^z = S_S^z\nabla T, \quad (85)$$

$$S_S^z = \frac{\hbar^2}{6\pi^2k_BT^2}\int dk\,k^2\left[\frac{e^{\hbar\omega_{\beta k}/k_BT}\,\omega_{\beta k}v_{\beta ky}^2}{\eta_{\beta k}(e^{\hbar\omega_{\beta k}/k_BT}-1)^2} - \frac{e^{\hbar\omega_{\alpha k}/k_BT}\,\omega_{\alpha k}v_{\alpha ky}^2}{\eta_{\alpha k}(e^{\hbar\omega_{\alpha k}/k_BT}-1)^2}\right], \quad (86)$$

where T is the average temperature and $\eta_{\mu k} = 1/\tau_{\mu k}$ is the μk-magnon relaxation rate. We consider the magnon and phonon systems to have the same temperature T. Equation (86) contains the most relevant dependencies of the SSE on the sample temperature and applied field. It shows, for instance, that in an easy-axis AF, the spin current, and hence the SSE, vanishes for $H = 0$, at any temperature, because the two modes have the same occupancy. In SSE experiments, one employs a metallic layer in contact with the AF layer, which is used to convert the spin current into a charge current by the inverse spin-Hall effect.[71] Using Eqs. (84)–(86), one can obtain the full expression for the spin current in the AF layer and calculate the fraction that is injected into the metallic layer to find the voltage that measures the spin Seebeck effect.[66,70]

VI. SUMMARY AND PERSPECTIVES

In this tutorial, we have presented a brief review of the basic concepts and properties of the collective spin excitations in antiferromagnets, the spin waves, whose quanta are called magnons. We have restricted attention to simple AF insulators with only two-sublattices, one class with easy-axis anisotropy, such as the fluorides MnF_2 and FeF_2, and the other with easy-plane anisotropy, such as NiO. For these materials, the magnon dispersion relations were calculated for the external magnetic field applied in different directions relative to the spins. Actually, antiferromagnets are known to exist with a great variety of crystalline structures and spin interactions, and new materials continue to be discovered in intense research efforts motivated by their promising future for spintronic applications.[10–14] The method used here to study magnons can be applied to AFs with more complex spin interactions, such as noncollinear antiferromagnets, where the chirality of the spin structure results in topological effects and opens up additional pathways for influencing transport phenomena.[72]

In regard to the excitation of magnons in antiferromagnets, we have discussed only one method, namely, the spin Seebeck effect, by which magnonic spin currents are generated by thermal gradients. Actually, magnons can be excited by several processes, such as spin current injection,[73] ultrafast optical excitation,[35,36] current driven dynamics produced by spin-transfer torque,[43] among others.[8–14] Thus, the experimental and theoretical study of magnonic phenomena in the wide variety of antiferromagnetic materials, known and yet to be discovered, constitutes a challenging and exciting field of research in magnetism and spintronics.

ACKNOWLEDGMENTS

This research was supported in Brazil by the Conselho Nacional de Desenvolvimento Científico e Tecnológico (CNPq), Coordenação de Aperfeiçoamento de Pessoal de Nível Superior (CAPES), Financiadora de Estudos e Projetos (FINEP), and Fundação de Amparo à Ciência e Tecnologia do Estado de Pernambuco (FACEPE), and in Chile by Fondo Nacional de Desarrollo Científico y Tecnológico (FONDECYT) No. 1170723.

REFERENCES

[1] L. Néel, "Influence des fluctuations des champs moléculaires sur les propriétés magnétiques des corps," Ann. Phys. **10**, 5 (1932).
[2] L. Néel, "Magnetism and local molecular field," Science **174**, 985 (1971).
[3] M. N. Baibich, J. M. Broto, A. Fert, F. N. Van Dau, F. Petroff, P. Etienne, G. Creuzet, A. Friederich, and J. Chazelas, "Giant magnetoresistance of (001)Fe/(001)Cr magnetic superlattices," Phys. Rev. Lett. **61**, 2472 (1988).
[4] G. Binasch, P. Grünberg, F. Saurenbach, and W. Zinn, "Enhanced magnetoresistance in layered magnetic structures with antiferromagnetic interlayer exchange," Phys. Rev. B **39**, 4828 (1989).
[5] B. Dieny, V. S. Speriosu, S. S. P. Parkin, B. A. Gurney, D. R. Wilhoit, and D. Mauri, "Giant magnetoresistive in soft ferromagnetic multilayers," Phys. Rev. B **43**, 1297 (1991).
[6] J. Nogués and I. K. Schuller, "Exchange bias," J. Magn. Magn. Mater. **192**, 203 (1999).
[7] J. R. Fermin, M. A. Lucena, A. Azevedo, F. M. de Aguiar, and S. M. Rezende, "Measurements of exchange anisotropy in NiFe/NiO films with different techniques," J. Appl. Phys. **87**, 6421 (2000).
[8] A. H. MacDonald and M. Tsoi, "Antiferromagnetic metal spintronics," Philos. Trans. R. Soc. A **369**, 3098 (2011).
[9] E. Gomonay and V. Loktev, "Spintronics of antiferromagnetic systems," Low Temp. Phys. **40**, 17 (2014).
[10] T. Jungwirth, X. Marti, P. Wadley, and J. Wunderlich, "Antiferromagnetic spintronics," Nat. Nano **11**, 231 (2016).
[11] O. Gomonay, T. Jungwirth, and J. Sinova, "Concepts of antiferromagnetic spintronics," Phys. Status Solidi RRL **11**, 1700022 (2017).
[12] M. B. Jungfleisch, W. Zhang, and A. Hoffmann, "Perspectives of antiferromagnetic spintronics," Phys. Lett. A **382**, 865 (2018).
[13] V. Baltz, A. Manchon, M. Tsoi, T. Moriyama, T. Ono, and Y. Tserkovnyak, "Antiferromagnetic spintronics," Rev. Mod. Phys. **90**, 015005 (2018).
[14] T. Jungwirth, J. Sinova, A. Manchon, X. Marti, J. Wunderlich, and C. Felser, "The multiple directions of antiferromagnetic spintronics," Nat. Phys. **14**, 200 (2018).
[15] L. J. de Jongh and A. R. Miedema, *Experiments on Simple Magnetic Model Systems* (Barnes & Noble Books, New York, 1974).
[16] F. Keffer and C. Kittel, "Theory of antiferromagnetic resonance," Phys. Rev. **85**, 329 (1952).
[17] T. Nagamiya, K. Yosida, and R. Kubo, *Antiferromagnetism, Advances in Physics* (Taylor & Francis, 1955).

[18]F. Keffer, "Spin waves," in *Handbuch der Physik* (Springer-Verlag, Berlin-Heidelberg, 1966), Vol. 18/2.
[19]O. Nikotin, P. A. Lindgard, and O. W. Dietrich, "Magnon dispersion relation and exchange interactions in MnF_2," J. Phys. C **2**, 1168 (1969).
[20]J. Barak, V. Jaccarino, and S. M. Rezende, "The magnetic anisotropy of MnF_2 at 0 K," J. Magn. Magn. Mater. **9**, 323 (1978).
[21]Y. Shapira and S. Foner, "Magnetic phase diagram of MnF_2 from ultrasonic and differential magnetization measurements," Phys. Rev. B **1**, 3083 (1970).
[22]S. M. Rezende, A. R. King, R. M. White, and J. P. Timbie, "Stability limit of the antiferromagnetic phase near the spin-flop boundary in MnF_2," Phys. Rev. B **16**, 1126 (1977).
[23]S. M. Wu, W. Zhang, K. C. Amit, P. Borisov, J. E. Pearson, J. S. Jiang, D. Lederman, A. Hoffmann, and A. Bhattacharya, "Antiferromagnetic spin Seebeck effect," Phys. Rev. Lett. **116**, 097204 (2016).
[24]R. C. Ohlmann and M. Tinkham, "Antiferromagnetic resonance in FeF_2 at Far-infrared frequencies," Phys. Rev. **123**, 425 (1961).
[25]M. T. Hutchings, B. D. Rainford, and H. J. Guggenheim, "Spin waves in antiferromagnetic FeF_2," J. Phys. C: Solid State Phys. **3**, 307 (1970).
[26]V. Jaccarino, A. R. King, M. Motokawa, T. Sakakibara, and M. Date, "Temperature dependence of FeF2 spin flop field," J. Magn. Magn. Mater. **31-34**, 1117 (1983).
[27]W. L. Roth, "Magnetic structures of MnO, FeO, CoO, and NiO," Phys. Rev. **110**, 1333 (1958).
[28]M. T. Hutchings and E. J. Samuelsen, "Measurement of spin-wave dispersion in NiO by inelastic neutron scattering and its relation to magnetic properties," Phys. Rev. B **6**, 3447 (1972).
[29]R. D. McMichael, M. D. Stiles, P. J. Chen, and W. F. Egelhoff, Jr., "Ferromagnetic resonance linewidth in thin films coupled to NiO," J. Appl. Phys. **83**, 7037 (1998).
[30]J. Nogués, *et al.*, "Isothermal tuning of exchange bias using pulsed fields," Appl. Phys. Lett. **82**, 3044 (2003).
[31]E. E. Fullerton and J. R. Childress, "Spintronics, magnetoresistive heads, and the emergence of the digital world," Proc. IEEE **104**, 1787 (2016).
[32]M. Grimsditch, L. E. McNeil, and D. J. Lockwood, "Unexpected behavior of the antiferromagnetic mode of NiO," Phys. Rev. B **58**, 14462 (1998).
[33]J. Milano, L. B. Steren, and M. Grimsditch, "Effect of dipolar interaction on the antiferromagnetic resonance spectra of NiO," Phys. Rev. Lett. **93**, 077601 (2004).
[34]A. J. Sievers III and M. Tinkham, "Far infrared antiferromagnetic resonance in MnO and NiO," Phys. Rev. **129**, 1566 (1963).
[35]T. Satoh, S.-J. Cho, R. Iida, T. Shimura, K. Kuroda, H. Ueda, Y. Ueda, B. A. Ivanov, F. Nori, and M. Fiebig, "Spin oscillations in antiferromagnetic NiO triggered by circularly polarized light," Phys. Rev. Lett. **105**, 077402 (2010).
[36]T. Kampfrath, *et al.*, "Coherent terahertz control of antiferromagnetic spin waves," Nat. Photon. **5**, 31 (2011).
[37]H. Wang, C. Du, P. Chris Hammel, and F. Yang, "Antiferromagnonic spin transport from $Y_3Fe_5O_{12}$ into NiO," Phys. Rev. Lett. **113**, 097202 (2014).
[38]C. Hahn, G. de Loubens, V. V. Naletov, J. Ben Youssef, O. Klein, and M. Viret, "Conduction of spin currents through insulating antiferromagnetic oxides," Europhys. Lett. **108**, 57005 (2014).
[39]H. Wang, C. Du, P. Chris Hammel, and F. Yang, "Spin transport in antiferromagnetic insulators mediated by magnetic correlations," Phys. Rev. B **91**, 220410 (R) (2015).
[40]T. Moriyama, S. Takei, M. Nagata, Y. Yoshimura, N. Matsuzaki, T. Terashima, Y. Tserkovnyak, and T. Ono, "Anti-damping spin transfer torque through epitaxial nickel oxide," Appl. Phys. Lett. **106**, 162406 (2015).
[41]W. Lin, K. Chen, S. Zhang, and C. L. Chien, "Enhancement of thermally injected spin current through an antiferromagnetic insulator," Phys. Rev. Lett. **116**, 186601 (2016).
[42]T. Shang, *et al.*, "Effect of NiO inserted layer on spin-hall magnetoresistance in Pt/NiO/YIG heterostructures," Appl. Phys. Lett. **109**, 032410 (2016).
[43]R. Cheng, D. Xiao, and A. Brataas, "Terahertz antiferromagnetic spin hall nano-oscillator," Phys. Rev. Lett. **116**, 207603 (2016).
[44]J. Holanda, D. S. Maior, O. Alves Santos, L. H. Vilela-Leão, J. B. S. Mendes, A. Azevedo, R. L. Rodríguez-Suárez, and S. M. Rezende, "Spin Seebeck effect in the antiferromagnet nickel oxide at room temperature," Appl. Phys. Lett. **111**, 172405 (2017).
[45]K. Kurosawa, M. Miura, and S. Saito, "Magnetic torque measurements on NiO (111) platelets," J. Phys. C Solid State Phys. **13**, 1521 (1980).
[46]I. Sänger, V. V. Pavlov, M. Bayer, and M. Fiebig, "Distribution of antiferromagnetic spin and twin domains in NiO," Phys. Rev. B **74**, 144401 (2006).
[47]F. L. A. Machado, P. R. T. Ribeiro, J. Holanda, R. L. Rodríguez-Suárez, A. Azevedo, and S. M. Rezende, "Spin-flop transition in the easy-plane antiferromagnet nickel oxide," Phys. Rev. B **95**, 104418 (2017).
[48]F. M. Johnson and A. H. Nethercot, Jr., "Antiferromagnetic resonance in MnF_2," Phys. Rev. **114**, 705 (1959).
[49]J. P. Kotthaus and V. Jaccarino, "Antiferromagnetic-Resonance linewidths in MnF_2," Phys. Rev. Lett. **28**, 1649 (1972).
[50]R. W. Sanders, D. Paquette, V. Jaccarino, and S. M. Rezende, "Radiation damping in magnetic resonance. II. continuous-wave antiferromagnetic-resonance experiments," Phys. Rev. B **10**, 132 (1974).
[51]M. Hagiwara, K. Katsumata, H. Yamaguchi, M. Tokunaga, I. Yamada, M. Gross, and P. Goy, "A complete frequency-field chart for the antiferromagnetic resonance in MnF_2," Int. J. Infrared Millim. Waves **20**, 617 (1999).
[52]R. W. Sanders, V. Jaccarino, and S. M. Rezende, "Magnetic polaritons, impurity mode enhancements and superradiance effects in FeF_2," Solid State Commun. **28**, 907 (1978).
[53]R. W. Sanders, R. M. Belanger, M. Motokawa, V. Jaccarino, and S. M. Rezende, "Far-infrared laser study of magnetic polaritons in FeF_2 and Mn impurity mode in FeF_2.Mn," Phys. Rev. B **23**, 1190 (1981).
[54]S. M. Rezende, R. L. Rodríguez-Suárez, and A. Azevedo, "Diffusive magnonic spin transport in antiferromagnetic insulators," Phys. Rev. B **93**, 054412 (2016).
[55]T. Holstein and H. Primakoff, "Field dependence of the intrinsic domain magnetization of a ferromagnet," Phys. Rev. **58**, 1098 (1940).
[56]S. M. Rezende and R. M. White, "Multimagnon theory of antiferromagnetic resonance relaxation," Phys. Rev. B **14**, 2939 (1976).
[57]R. M. White, *Quantum Theory of Magnetism*, 3rd ed. (Springer-Verlag, Berlin, Heidelberg, 2007).
[58]S. P. Bayrakci, T. Keller, K. Habicht, and B. Keimer, "Spin-Wave lifetimes throughout the brillouin zone," Science **312**, 1926 (2006).
[59]S. M. Rezende and R. M. White, "Spin wave lifetimes in antiferromagnetic $RbMnF_3$," Phys. Rev. B **18**, 2346 (1978).
[60]T. Oguchi, "Theory of spin-wave interactions in ferro- and antiferromagnetism," Phys. Rev. **117**, 117 (1960).
[61]R. M. White, M. Sparks, and I. Ortenburger, "Diagonalization of the antiferromagnetic magnon-phonon interaction," Phys. Rev. **139**, A450 (1965).
[62]S. M. Rezende and N. Zagury, "Coherent magnon states," Phys. Lett. A **29**, 47 (1969).
[63]N. Zagury and S. M. Rezende, "Theory of macroscopic excitations of magnons," Phys. Rev. B **4**, 201 (1971).
[64]Y. Kajiwara, K. Harii, S. Takahashi, J. Ohe, K. Uchida, M. Mizuguchi, H. Umezawa, K. Kawai, K. Ando, K. Takanashi, S. Maekawa, and E. Saitoh, "Transmission of electrical signals by spin-wave interconversion in a magnetic insulator," Nature **464**, 262 (2010).
[65]S. S.-L. Zhang and S. Zhang, "Magnon mediated electric current drag across a ferromagnetic insulator layer," Phys. Rev. Lett. **109**, 096603 (2012).
[66]S. M. Rezende, A. Azevedo, and R. L. Rodríguez-Suárez, "Magnon diffusion theory for the spin Seebeck effect in ferromagnetic and antiferromagnetic insulators," J. Phys. D Appl. Phys. **51**, 174004 (2018).
[67]G. E. W. Bauer, E. Saitoh, and B. J. van Wees, "Spin caloritronics," Nat. Mater. **11**, 391 (2012).
[68]S. R. Boona, R. C. Myers, and J. P. Heremans, "Spin caloritronics," Energy Environ. Sci. **7**, 885 (2014).

[69]K. Uchida, H. Adachi, T. Kikkawa, A. Kirihara, M. Ishida, S. Yorozu, S. Maekawa, and E. Saitoh, "Thermoelectric generation based on spin Seebeck effects," Proc. IEEE **104**, 1946 (2016).
[70]S. M. Rezende, R. L. Rodríguez-Suárez, and A. Azevedo, "Theory of the spin Seebeck effect in antiferromagnets," Phys. Rev. B **93**, 014425 (2016).
[71]A. Hoffmann, "Spin hall effects in metals," IEEE Trans. Magn. **49**, 5172 (2013).
[72]C. Sürgers, G. Fischer, P. Winkel, and H. V. Löhneysen, "Large topological hall effect in the non-collinear phase of an antiferromagnet," Nat. Commun. **5**, 3400 (2014).
[73]R. Lebrun, A. Ross, S. A. Bender, A. Qaiumzadeh, L. Baldrati, J. Cramer, A. Brataas, R. A. Duine, and M. Kläui, "Tunable long-distance spin transport in a crystalline antiferromagnetic iron oxide," Nature **561**, 222 (2018).